Biochemical Pharmacology 242 (2025) 117420

Contents lists available at ScienceDirect

Biochemical Pharmacology

journal homepage: www.elsevier.com/locate/biochempharm

Zaltoprofen and its novel analogues exhibit dual targeting of COX-2 and PPAR-γ, providing a strategy to alleviate lipopolysaccharide – induced acute lung injury

Qirong Lu [a], Yongxia Zhao [b], Xiaoqing Xu [b], Pu Guo [a,b], Irma Ares [c], Marta Martínez [c], Bernardo Lopez-Torres [c], María-Rosa Martínez-Larrañaga [c], Arturo Anadón [c,*], Yuanhu Pan [b,d,**], Xu Wang [b,d,**], María-Aránzazu Martínez [c]

[a] Hubei Key Laboratory of Animal Nutrition and Feed Science, School of Animal Science and Nutritional Engineering, Wuhan Polytechnic University, Wuhan 430023, China
[b] National Reference Laboratory of Veterinary Drug Residues (HZAU) and MAO Key Laboratory for Detection of Veterinary Drug Residues, Huazhong Agricultural University, Wuhan, Hubei 430070, China
[c] Department of Pharmacology and Toxicology, Faculty of Veterinary Medicine, Universidad Complutense de Madrid, Madrid 28040, Spain
[d] MOA Laboratory for Risk Assessment of Quality and Safety of Livestock and Poultry Products, Hubei 430070, China

ARTICLE INFO

Keywords:
Acute lung injury
Dual target
Cyclooxygenase-2
Peroxisome proliferator-activated receptor-γ
Zaltoprofen
Strategy

ABSTRACT

Acute lung injury (ALI) is a multi-system and multifactorial disease, which is characterised by an uncontrolled inflammatory response and high mortality. Zaltoprofen (ZPF), is a non-steroidal anti-inflammatory drug (NSAID) with powerful anti-inflammatory effects, as well as an analgesic action on inflammatory pain. Therefore, this research study aims to explore whether ZPF, its main metabolite M2 (S-oxide-zaltoprofen) and novel analogues can alleviate ALI through multiple targets. Based on molecular docking, the similar topological structure binding properties of protein targets (STSBPT) strategy, the cellular thermal shift assay (CETSA) and drug affinity

Abbreviations: ^{1}H NMR, proton nuclear magnetic resonance spectroscopy; AA, amino acid; ALI, acute lung injury; ARDS, acute respiratory distress syndrome; Arg120, arginine 120; Arg288, arginine 288; BCA, bicinchoninic acid; BSA, bovine serum albumin; CCK-8, cell counting kit-8; CETSA, cellular thermal shift assay; COX-1, cyclooxygenase-1; COX-2, cyclooxygenase-2; D63, 10,11-dihydro-α-methyl-10-oxodibenzo[*b*,*f*]thiepin-2-acetic acid 2- (2-thienylmethylene)hydrazide; DARTS, drug affinity responsive target stability; DMEM, Dulbecco's modified eagle medium; DMF, dimethylformamide; DMSO, dimethyl sulfoxide; DMAP, 4-dimethylaminopyridine; E63, dibenzo[*b*,*f*]thiepin-2-acetic acid, α-methyl-, 2-(2-thienylmethylene)hydrazide, 5-oxide; EDC, 1-Ethyl-3-[3-(dimethylamino)propyl] carbodiimide; ERK, extracellular signal-regulated kinase; ERK1/2, extracellular signal-regulated kinase 1/2; GAPDH, glyceraldehyde-3-phosphate dehydrogenase; GW9662, 2-chloro-5-nitrobenzanilide; H_2SO_4, sulfuric acid; H_2O_2, hydrogen peroxide; H3, histone H3; HBSS, Hank's balanced salt solution; HCl, hydrochloric acid; IL-1β, interleukin-1β; i-NOS, inducible nitric oxide synthase; IκBα, NF-κB inhibitor alpha; JC2/JMC2, dibenzo[*b*,*f*]thiepin-2-acetic acid, α-methyl-3-[5-oxide-4-(phenylsulfonyl) −1,2,5-oxadiazol-3-yl]oxy]propyl ester, 5-oxide (ACI); JC5/JMC5, dibenzo[*b*,*f*]thiepin-2-acetic acid, 10,11-dihydro-α-methyl-10-oxo-, 3-[5-oxide-4-(phenylsulfonyl)-1,2,5-oxadiazol-3-yl]oxy]propyl ester (ACI); JC6/JMC6, dibenzo[*b*,*f*]thiepin-2-acetic acid, 10,11-dihydro-α-methyl-10-oxo-, 3-[5-oxide-4-(phenylsulfonyl)-1,2,5-oxadiazol-3-yl]oxy]propyl ester, 5-oxide (ACI); JNK, c-Jun N-terminal protein kinase; Leu288, leucine 288; LOX, lipoxygenase; LPS, lipopolysaccharide; M2, S-oxide-zaltoprofen; M282, dibenzo[*b*,*f*]thiepin-2-acetic acid, α-methyl- (9CI, ACI); M3, 10-hydroxy-zaltoprofen; M5, S-oxide-10-hydroxy-zaltoprofen; M6, dibenzo[*b*,*f*]thiepin-2-acetic acid, α-methyl-, 5-oxide (ACI); MAPK, mitogen-activated protein kinase; Mof, mofezolac; $NaBH_4$, sodium borohydride; Na_2SO_4, sodium sulfate anhydrous; NF-κB p65, nuclear factor kappa B p65; NF-κB, nuclear factor kappa B; NHS, N-hydroxysuccinimide; NLRP3, NOD-like receptor thermal protein domain associated protein 3; NSAID, non-steroidal anti-inflammatory drug; p38 MAPK, mitogen-activated protein kinase p38; p38, mitogen-activated protein kinase 14; p65, nuclear factor NF-kappa-B p65 subunit; PBS, phosphate buffered saline; PDB, 4XTA, PPAR-γ crystal; PDB, 5IKQ, COX-2 crystal; p-ERK, phosphorylated extracellular signal-regulated kinase; PGE2, prostaglandin E2; p-IκBα, phosphorylated NF-κB inhibitor alpha; p-JNK, phosphorylated c-Jun N-terminal protein kinase; p-NF-κB p65, phosphorylated nuclear factor kappa B p65; p-p38, phosphorylated p38; p-p65, phosphorylated p65; PPAR-γ, peroxisome proliferator-activated receptor-γ; PVDF, polyvinylidene difluoride; PyMOL, a cross-platform molecular graphics system; Ser342, serine 342; Ser530, serine 530; SPF, specific pathogen-free; STSBPT, similar topological structure binding properties of protein targets; TBST, tween 20/Tris-buffered saline; TLR4-MD2, Toll-like receptor 4-myeloid differentiation factor 2; TNF-α, tumor necrosis factor-α; Tyr355, tyrosine 355; ZPF, zaltoprofen; ZPF/M2, zaltoprofen/ S-oxide-zaltoprofen.

* Corresponding author at: Universidad Complutense de Madrid (UCM). 28040 Madrid, Spain.
** Corresponding authors at: National Reference Laboratory of Veterinary Drug Residues (HZAU) and MAO Key Laboratory for Detection of Veterinary Drug Residues, Huazhong Agricultural University, Wuhan, Hubei 430070, China.
E-mail addresses: aanadon@ucm.es (A. Anadón), panyuanhu@mail.hzau.edu.cn (Y. Pan), wangxu@mail.hzau.edu.cn (X. Wang).

https://doi.org/10.1016/j.bcp.2025.117420
Received 2 December 2024; Received in revised form 20 May 2025; Accepted 9 October 2025
Available online 11 October 2025
0006-2952/© 2025 The Author(s). Published by Elsevier Inc. This is an open access article under the CC BY license (http://creativecommons.org/licenses/by/4.0/).

responsive target stability (DARTS), for first time, this study found that cyclooxygenase-2 (COX-2) and peroxisome proliferator-activated receptor-γ (PPAR-γ) are dual targets of ZPF and M2. Based on this outcome, novel analogues related to ZPF and M2 were designed. The present research study also examined the effect and the cellular and molecular mechanisms of ZPF, M2 and the novel analogues on LPS-induced ALI *in vitro* and *in vivo*, through the dual targets of COX-2 and PPAR-γ. The findings of this study suggest that the STSBPT strategy could assist as a probable multi-target medicinal drug screening strategy, and ZPF, its main metabolite M2 and its novel analogues could serve as potential therapeutic agents for the treatment of ALI, through the both COX-2 and PPAR-γ molecular signalling targets.

1. Introduction

The interaction between medicinal drugs and multi-targets is an important technology in the development of new medicines and in the improvement of their efficacy. Despite significant progress in pharmaceutical technology and increased global research funding, the field of medicinal chemistry, which is concerned with drug design and the synthesis of biologically active molecules, is in crisis, mainly reflected in the low number of novel medicinal drug approvals per year [1]. One major challenge in developing new medicines stems, at least in part, from the inherent limitations of the traditional "single-target" strategy [2]. Conventional medicinal drugs are largely designed to address single-gene disorders by targeting a specific protein or molecular signaling pathway. However, the occurrence and development of many clinical diseases presents a multifactorial etiology, and an efficient multi-target network regulation mode [3,4]. This highlights an urgent need to shift drug development strategies toward a multi-target drug design paradigm. Supporting this approach, many clinically effective medicines demonstrate multi-target therapeutic effects, meaning they interact with multiple proteins to exert their pharmacological actions [1,5]. Consequently, targeting multiple pathways of a specific disease may offer a more effective treatment strategy than focusing on a single target [6]. A notable example is the novel class of dual acting non-steroidal anti-inflammatory drugs (NSAIDs) called COX/LOX competitive inhibitors, in particular "licofelone" (which decreases the production of proinflammatory leukotrienes and prostaglandins) developed to treat osteoarthritis after the selective single target-cyclooxygenase-2 (COX-2) inhibitor rofecoxib was voluntarily withdrawn from the pharmaceutical market due to safety concerns regarding myocardial infarction and stroke. Consequently, this offered a silver lining to the successful design of medicines based on multiple targets [7,8], suggesting that multi-target drugs may have a potential advantage over single target drugs in terms of both treatment and safety issues. While the multi-target drug approach is gaining traction for treating complex diseases, a significant challenge lies in the inability to effectively predict the outcomes of this approach, which has contributed to its slow progress. To address this issue, this research study proposes a novel strategy to predict closely related targets based on the similarity in spatial structure of the medicinal drug targets, thus overcoming the difficulties of the multi-target approach, as well as solving the key scientific problems. As each medicinal drug that binds to the target protein has a unique active binding pocket, it is possible to judge whether the medicinal drug has multiple targets by assessing the similarity of the topological structure of the protein active binding pocket, namely the "similar topological structure binding properties of protein targets" (STSBPT) strategy, provides a theoretical basis for the development of new drugs.

Acute lung injury (ALI) and severe forms of acute respiratory distress syndrome (ARDS) are clinical syndromes with diverse causes and alarmingly high mortality rates. They are characterised by an uncontrolled inflammatory response, increased alveolar capillary barrier penetration, and pulmonary oedema, among other clinical symptoms [9,10]. Although great progress has been made in improving the supportive care for ARDS, an effective pharmacological treatment has not been established, and its fatality rate remains distressingly high at 30–40 % [11]. Furthermore, ALI can induce destructive hypoxia and ischemic stress or the release of bacterial endotoxins [such as lipopolysaccharide (LPS)]. The LPS-induced lung inflammation model has become a widely used tool for investigating the acute inflammatory response in ALI following exposure [10,12]. ALI, being a multifaceted system and a multi-target disease, presents the possibility of treatment through the development of multi-target drugs.

Zaltoprofen (ZPF) ((+/−)-2-(10,11-dihydro-10-oxo-dibenzo[b,f] thiepin-2-yl)- propionic acid), $C_{17}H_{14}O_3S$, 74711–43-6) is a preferential cyclooxygenase-2 (COX-2) inhibitor known for its robust anti-inflammatory and analgesic effects on inflammatory pain [13]. This indicates its potential applicability in the treatment of ALI, although further research is necessary to confirm whether it exhibits multi-target properties. In humans, ZPF is metabolised to S-oxide-zaltoprofen (M2), 10-hydroxy-zaltoprofen (M3) and S-oxide-10-hydroxy-zaltoprofen (M5) [14]. Compared to other NSAIDs, such as pranoprofen (2-(5H-chromeno [2,3-b] pyridin-7-yl)propanoic acid, $C_{15}H_{13}NO_3$, 52549–17-4) (an NSAID used in ophthalmology) and indomethacin (an NSAID used for the treatment of inflammation and pain), ZPF causes the preferential potent inhibition of COX-2, exhibits a potent inhibitory action on the nociceptive responses induced by a retrograde infusion of bradykinin into the right common carotid artery in rats [15], and has fewer adverse events on the gastrointestinal tract [16,17]. Since many NSAIDs are metabolised into active metabolites within the body, it is crucial to investigate the anti-inflammatory effect of ZPF's active metabolites, as this will help to better understand the mechanism of action of this pharmacologically active substance. Additionally, exploring whether ZPF or its active metabolites act on other anti-inflammatory targets beyond COX-2 remains an area of interest that warrants further investigation. The STSBPT strategy, which is grounded in multi-target drug development, offers a valuable approach for predicting alternative anti-inflammatory targets of ZPF and its active metabolites. These predicted targets could share functional similarities with COX-2, providing a broader perspective on the compound's therapeutic potential.

As mentioned previously, ALI is a highly fatal disease characterized by its involvement of multiple complex systems and diverse molecular signaling pathways, closely linked to inflammation. Despite advances in pharmacological research, current treatments fail to significantly alleviate lung injury or reduce ALI-related mortality [18,19]. ZPF is an anti-inflammatory and analgesic drug with multiple molecular signalling targets, implying that it may be a potential multi-target drug for the treatment of ALI. Meanwhile, the design of multi-target drugs has significant advantages in the treatment of multisystem complex diseases compared to single target medicinal drugs. Therefore, in this research study, the STSBPT strategy was used to screen another critical anti-inflammatory target of ZPF, M2 and its novel analogues: peroxisome proliferator-activated receptor-γ (PPAR-γ). This was fully validated by the cellular thermal shift assay (CETSA) and drug affinity responsive target stability (DARTS). Furthermore, novel analogues were designed based on the multi-target perspective of the STSBPT strategy, and the efficacy of ZPF, M2 and its novel analogues was evaluated against LPS-induced ALI both *in vitro* and *in vivo*. In summary, ZPF, its main metabolite M2 and its novel analogues could serve as potential therapeutic agents for ALI treatment through the dual target molecular signalling of COX-2 and PPAR-γ. These findings not only highlight new

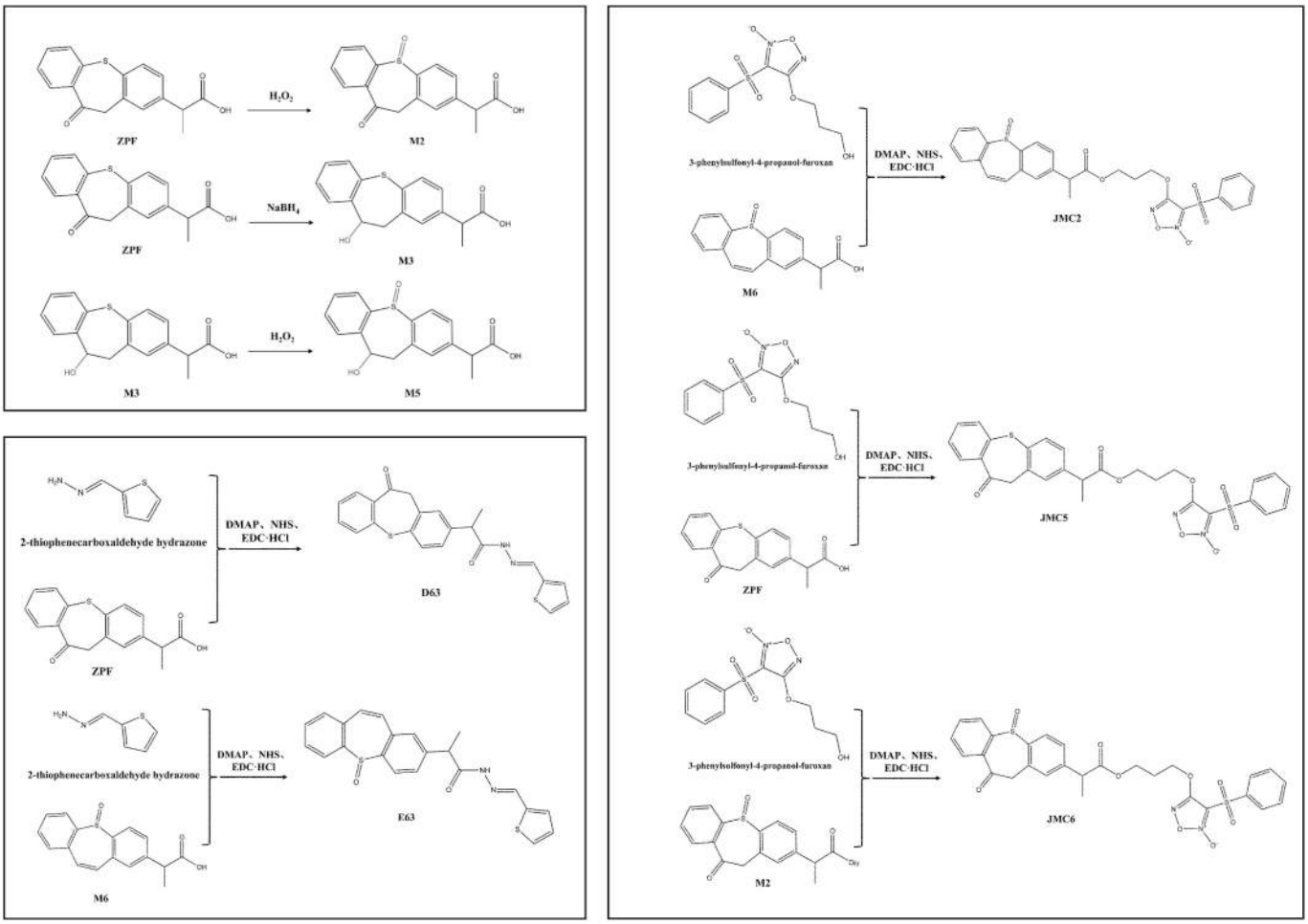

Fig. 1. Schematic pathways for the synthesis of the metabolites (M2, M3 and M5) and novel analogues (D63, E63, JMC2, JMC5 and JMC6) of ZPF.

multi-target screening strategies and therapeutic targets but also lay the groundwork for developing novel NSAIDs to mitigate inflammatory injury. This approach has the potential to reduce the incidence of ALI and its devastating consequences.

2. Materials and methods

2.1. Chemistry

ZPF (99 %) was purchased from ShangHai YuanYe Biotechnology (Shanghai, China). Zaltoprofen metabolites and analogues: M2 (S-oxide-zaltoprofen) (95 %), M3 (10-hydroxy-zaltoprofen) (95 %) M5 (S-oxide-10-hydroxy-zaltoprofen) (95 %) D63 (10,11-dihydro-α-methyl-10-oxo-dibenzo[*b*,*f*]thiepin-2-acetic acid 2-(2-thienylmethylene)hydrazide) (95 %), E63 (dibenzo[*b*,*f*]thiepin-2-acetic acid, α-methyl-2-(2-thienyl-methylene)hydrazide, 5-oxide) (95 %), JMC2 (dibenzo[*b*,*f*]thiepin-2-acetic acid, α-methyl-3-[5-oxide-4-(phenylsulfonyl)-1,2,5-oxadiazol-3-yl]oxy]propyl ester, 5-oxide (ACI)) (95 %), JMC5 (dibenzo[*b*,*f*]thiepin-2-acetic acid, 10,11-dihydro-α-methyl-10-oxo- 3-[5-oxide-4-(phenylsulfonyl)-1,2,5-oxadiazol-3-yl]oxy]propyl ester (ACI) (95 %), JMC6 (dibenzo[*b*,*f*]thiepin-2-acetic acid, 10,11-dihydro-α-methyl-10-oxo- 3-[5-oxide-4-(phenylsulfonyl)-1,2,5-oxadiazol-3-yl]oxy]propyl ester, 5-oxide (ACI) (95 %), were synthesized by the Institute of Veterinary Pharmaceuticals (Huazhong Agricultural University, Wuhan, PR China). In addition, chemical synthesis related reagents were purchased from Sinopharm Chemical Reagent Co., Ltd (Shanghai, China).

The schematic pathways for the synthesis of metabolites (M2, M3, M5) and novel analogues (D63, E63, JMC2, JMC5, JMC6) of ZPF are presented in Fig. 1. Moreover, characteristic analysis (^{1}H NMR data) to confirm ZPF and synthesized metabolites, as well as the synthesized novel analogues is presented in Fig. 2 and Fig. 3, respectively.

2.1.1. Preparation of metabolite M2 (S-oxide-zaltoprofen)

To a solution of ZPF (2.98 g) in acetic acid (25 mL) 30 % hydrogen peroxide (H_2O_2) (1 mL) was added dropwise at 25 °C, and the mixture was stirred for 5 h at 45 °C. After the reaction was completed, the reaction mixture was poured into ice-water and the formed crude product was collected by filtration [20]. The target product was obtained by column chromatography on silica gel using petroleum ether/ethyl acetate (1.5:1) as the eluent and then recrystallized from ethyl acetate/methanol to yield a white solid product.

2.1.2. Preparation of metabolite M3 (10-hydroxy-zaltoprofen)

To a solution of ZPF (5.96 g) in dry methanol (100 mL) sodium borohydride ($NaBH_4$) was added at 25 °C, and the mixture was stirred for 2 h at 45 °C [21]. After the reaction was completed, the mixture was cooled to room temperature and 5 % aqueous HCl was added to adjust the pH to 4. The solvent was removed under reduced pressure and extracted with ethyl acetate (3 × 50 mL), then the combined organic layer was washed with water, dried over Na_2SO_4 and evaporated under reduced pressure to afford a crude M3, which was purified by column chromatography on silica gel using dichloromethane/methanol (20:1) complemented with 0.5 % acetic acid as the eluent to yield a white powder product.

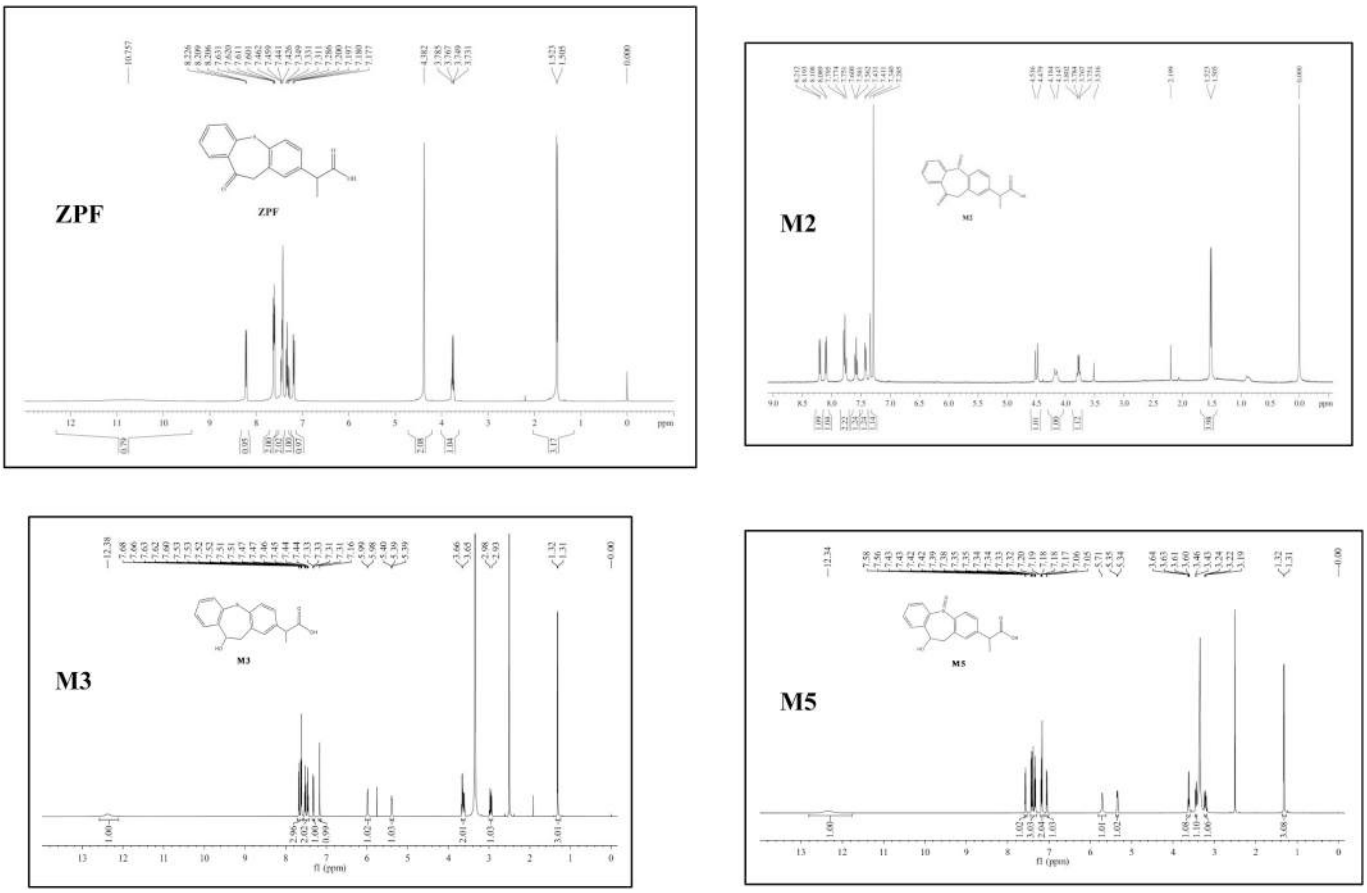

Fig. 2. ^{1}H NMR data of ZPF and its metabolites (M2, M3 and M5). **ZPF:** White solid. ^{1}H NMR (400 MHz, $CDCl_3$) δ 10.76 (s, 1H), 8.21 (d, J = 6.8 Hz, 1H), 7.62 (q, 4.4 Hz, 2H), 7.45 (t, 6.0 Hz, 2H), 7.35 – 7.29 (m, 1H), 7.19 (q, 1.2 Hz, 1H), 4.38 (s, 2H), 3.76 (q, 7.2 Hz, 1H), 1.51 (d, J = 7.2 Hz, 3H). **M2:** White solid. 8.20 (d, J = 7.6 Hz, 1H), 8.10 (d, J = 7.6 Hz, 1H), 7.77 (t, J = 8.4, 9.2 Hz, 2H), 7.58 (t, J = 7.6 Hz, 1H), 7.42 (d, J = 8.0 Hz, 1H), 7.34 (s, 1H), 4.50 (d, J = 14.8 Hz, 1H), 4.17 (d, J = 14.8 Hz, 1H), 3.78 (q, 7.2 Hz, 1H), 1.51 (d, J = 7.2 Hz, 3H). **M3**: White solid. ^{1}H NMR (600 MHz, DMSO) δ 12.38 (s, 1H), 7.68 – 7.60 (m, 3H), 7.53 – 7.44 (m, 2H), 7.32 (d, J = 12.0 Hz, 1H), 7.16 (s, 1H), 5.98 (d, J = 6.0 Hz, 1H), 5.40 (t, J = 6.0 Hz, 1H), 3.66 – 3.61 (m, 2H), 2.98 – 2.93 (m, 1H), 1.31 (d, J = 6.0 Hz, 3H). **M5**: White solid. ^{1}H NMR (600 MHz, DMSO) δ 12.34 (s, 1H), 7.57 (d, 12.0 Hz, 1H), 7.43 – 7.32 (ddm, 6.0, 6.0 Hz, 3H), 7.20 – 7.17 (m, 2H), 7.06 (d, 6.0 Hz, 1H), 5.71 (s, 1H), 5.35 (d, 6.0 Hz, 1H), 3.62 (q, 6.0 Hz, 1H), 3.45 (d, 18.0 Hz, 1H), 3.24 – 3.19 (m, 1H), 1.32 (d, 6.0 Hz, 3H).

2.1.3. Preparation of metabolite M5 (S-oxide-10-hydroxy-zaltoprofen)

To a solution of M3 (1.57 g) in acetic acid (25 mL) 30 % hydrogen peroxide (H_2O_2) (1 mL) was added dropwise at 25 °C, and the mixture was stirred for 5 h at 45 °C. After the reaction was completed, the reaction mixture was extracted with ethyl acetate (3 × 50 mL), then the combined organic layer was washed with water, dried over Na_2SO_4 and evaporated under reduced pressure to afford a crude product, which was purified by column chromatography on silica gel using dichloromethane/methanol/acetic acid (100:3:1) as the eluent to yield a white solid product [20].

2.1.4. Preparation of M282 (dibenzo[b,f]thiepin-2-acetic acid, α-methyl-(9CI, ACI)

To a solution of M3 (5 g) in acetic acid (40 mL) H_2SO_4 (3 mL) was added dropwise at 25 °C. The mixture was stirred at 25 °C for 15 min, and then stirred at 45 °C for 15 min. Adding sodium hydroxide (1 mol/L) to adjust the pH to 5–6 after the reaction. The reaction mixture was extracted with ethyl acetate (3 × 100 mL), and then the combined organic layer was washed with water, dried over Na_2SO_4 and evaporated under reduced pressure to afford a crude product [21,22].

2.1.5. Preparation of M6 (dibenzo[b,f]thiepin-2-acetic acid, α-methyl-, 5-oxide (ACI)

To a solution of M282 (2 g) in acetic acid (25 mL) 30 % hydrogen peroxide (H_2O_2) (1 mL) was added dropwise at 25 °C, and the mixture was stirred at 45 °C for 5 h [20]. Sodium hydroxide (1 mol/L) was added to adjust the pH to 5–6 after the reaction. The reaction mixture was extracted with ethyl acetate (3 × 100 mL), and then the combined organic layer was washed with water, dried over Na_2SO_4 and evaporated under reduced pressure to afford a crude product, which was purified by column chromatography on silica gel using dichloromethane/methanol (20:1) complemented with 0.5 % acetic acid as the eluent to yield a white solid product.

2.1.6. Preparation of 3-phenylsulfonyl-4-propanol-furoxan

To a solution of 3,4-bis(phenylsulfonyl)furoxan (2 g) in tetrahydrofuran (20 mL) 1,3-propanediol (3 g) was added, and then 25 % NaOH (1 mL) was added as the catalyst [23]. The mixture was stirred at 40 °C for 4 h. The solvent was removed under reduced pressure and extracted with ethyl acetate (3 × 50 mL), then the combined organic layer was washed with water, dried over Na_2SO_4 and evaporated under reduced pressure to afford a crude M3, which was purified by column chromatography on silica gel using petroleum ether: ethyl acetate (3:2) as the eluent to yield a white powder product.

2.1.7. Preparation of 2-thiophenecarboxaldehyde hydrazine

To a solution of 2-thienaldehyde (1.5 mL) in tetrahydrofuran (7 mL), hydrazine hydrate (1 mL) was added dropwise, and the mixture was stirred at 25 °C. After the reaction was completed, the solvent was removed under reduced pressure to afford a white solid product, which

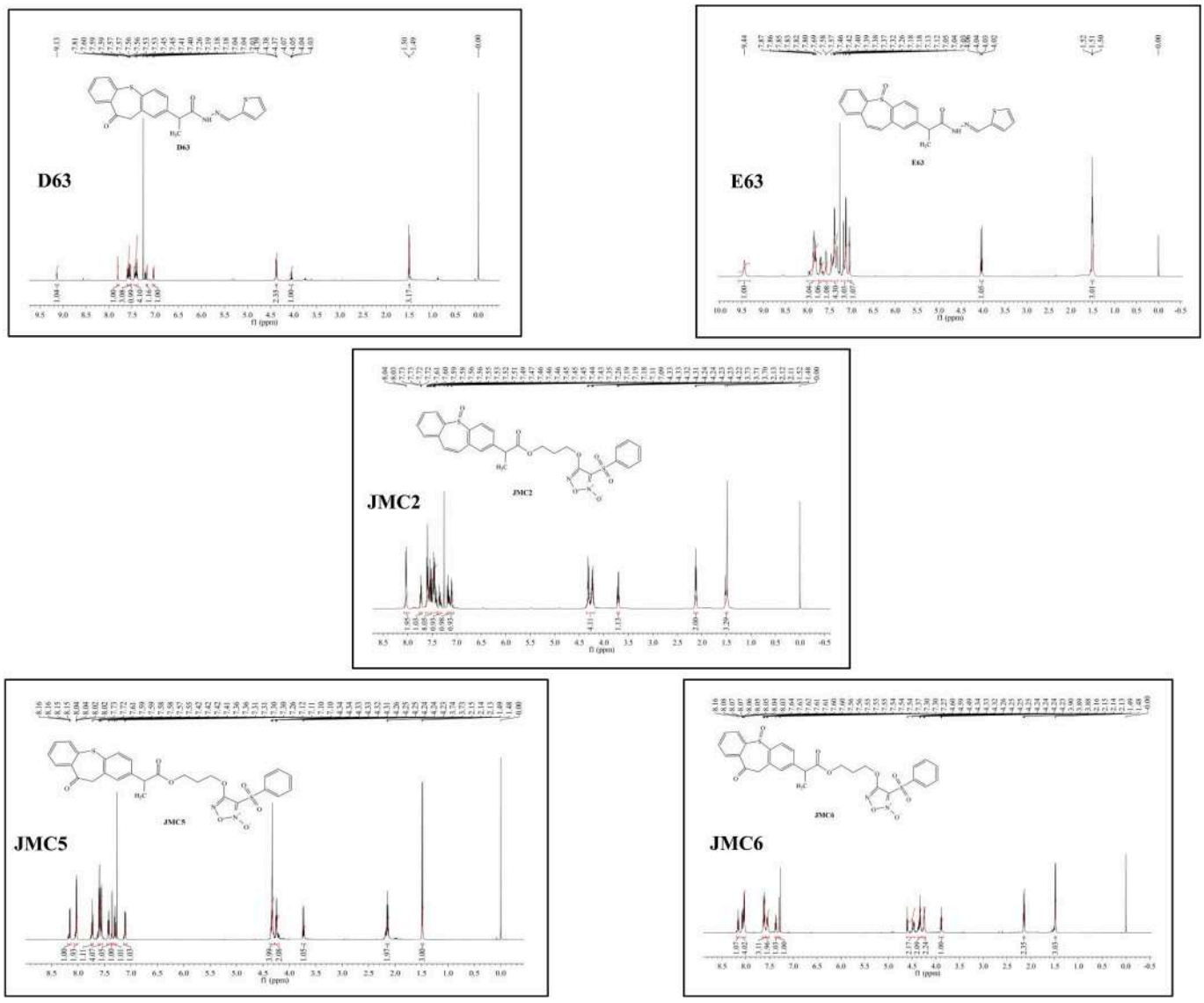

Fig. 3. ^{1}H NMR data of novel analogues (D63, E63, JMC2, JMC5 and JMC6) of ZPF. **D63:** White solid. ^{1}H NMR (600 MHz, $CDCl_3$) δ 9.13 (s, 1H), 7.81 (s, 1H), 7.61 – 7.55 (m, 3H), 7.53 (d, J = 1.7 Hz, 1H), 7.46 – 7.38 (m, 4H), 7.18 (dd, J = 3.6, 0.7 Hz, 1H), 7.04 (dd, J = 5.1, 3.6 Hz, 1H), 4.39 – 4.36 (m, 2H), 4.05 (q, J = 7.2 Hz, 1H), 1.50 (d, J = 7.1 Hz, 3H). **E63:** White solid. ^{1}H NMR (600 MHz, $CDCl_3$) δ 9.44 (s, 1H), 8.00 – 7.75 (m, 3H), 7.75 – 7.63 (m, 1H), 7.58 (dd, J = 10.7, 7.2 Hz, 1H), 7.48 – 7.31 (m, 4H), 7.23 – 7.07 (m, 3H), 7.07 – 7.00 (m, 1H), 4.04 (q, J = 7.2 Hz, 1H), 1.51 (t, J = 7.0 Hz, 3H). **JMC2:** Yellow oil. ^{1}H NMR (600 MHz, $CDCl_3$) δ 8.03 (d, J = 8.3 Hz, 2H), 7.73 (td, J = 7.6, 0.9 Hz, 1H), 7.63 – 7.40 (m, 8H), 7.35 (t, J = 7.5 Hz, 1H), 7.18 (dd, J = 12.0, 4.3 Hz, 1H), 7.10 (dt, J = 8.1, 2.1 Hz, 1H), 4.35 – 4.19 (m, 4H), 3.71 (dd, J = 15.8, 8.6 Hz, 1H), 2.12 (p, J = 6.1 Hz, 2H), 1.50 (d, J = 7.2 Hz, 3H). **JMC5:** White solid. ^{1}H NMR (600 MHz, $CDCl_3$) δ 8.15 (dd, J = 8.0, 1.5 Hz, 1H), 8.07 – 8.00 (m, 2H), 7.75 – 7.71 (m, 1H), 7.58 (ddd, J = 17.5, 8.1, 6.0 Hz, 4H), 7.45 – 7.40 (m, 1H), 7.36 (d, J = 1.8 Hz, 1H), 7.30 (td, J = 7.8, 1.2 Hz, 1H), 7.12 (ddd, J = 12.4, 8.0, 1.9 Hz, 1H), 4.37 – 4.28 (m, 4H), 4.24 (qt, J = 11.4, 5.7 Hz, 2H), 3.73 (q, J = 7.1 Hz, 1H), 2.18 – 2.11 (m, 2H), 1.49 (d, J = 7.2 Hz, 3H). **JMC6:** White solid. ^{1}H NMR (600 MHz, $CDCl_3$) δ 8.19 – 8.14 (m, 1H), 8.06 (ddd, J = 14.2, 12.0, 8.2 Hz, 4H), 7.64 – 7.59 (m, 3H), 7.58 – 7.51 (m, 2H), 7.39 – 7.34 (m, 1H), 7.30 (d, J = 0.7 Hz, 1H), 4.62 – 4.44 (m, 2H), 4.38 – 4.31 (m, 2H), 4.25 (ddd, J = 6.2, 3.9, 1.7 Hz, 2H), 3.89 (t, J = 5.8 Hz, 1H), 2.14 (dd, J = 11.8, 5.9 Hz, 2H), 1.49 (d, J = 7.2 Hz, 3H).

was pure enough to proceed to the next steps without further purification [24].

2.1.8. General procedure for the synthesis of JMC2 (dibenzo[b,f]thiepin-2-acetic acid, α-methyl-, 3-[[5-oxido-4-(phenylsulfonyl)-1,2,5-oxadiazol-3-yl]oxy]propyl ester, 5-oxide (ACI), JMC5 (dibenzo[b,f]thiepin-2-acetic acid, 10,11-dihydro-α-methyl-10-oxo-,3- [[5-oxido-4-(phenylsulfonyl)-1,2,5-oxadiazol-3-yl]oxy]propyl ester (ACI) and JMC6 (dibenzo[b,f] thiepin-2-acetic acid, 10,11-dihydro-α-methyl-10-oxo-,3- [[5-oxido-4-(phenylsulfonyl)-1,2,5-oxadiazol-3-yl]oxy]propyl ester, 5-oxide (ACI)

To a solution of M6/ZPF/M2 (1.3 mmol) in dimethylformamide (DMF), the corresponding 4-dimethylaminopyridine (DMAP) (3.9 mmol), N-hydroxysuccinimide (NHS) (2.6 mmol) and 1-ethyl-3-(3-dimethylaminopropyl) carbodiimide hydrochloride (EDC·HCl) (2.6 mmol) were added, and the mixture was stirred at 35 °C for 2 h, after which 3-phenylsulfonyl-4-propanol-furoxan (1.5 mmol) was added to the reaction mixture. After the reaction was completed, the solvent was removed under reduced pressure and extracted with ethyl acetate (3 × 30 mL), then the combined organic layer was washed with water, dried over Na_2SO_4 and evaporated under reduced pressure to afford crude M3, which was purified by column chromatography on a silica gel using dichloromethane/methanol (20:1) complemented with 0.5 % acetic acid as the eluent to yield the product [25].

2.1.9. General procedure for the synthesis of D63 (10,11-dihydro-α-methyl-10-oxodibenzo[b,f]thiepin-2-acetic acid 2-(2-thienylmethylene) hydrazide) and E63 (dibenzo[b,f]thiepin-2-acetic acid, α-methyl-, 2-(2-thienylmethylene)hydrazide, 5-oxide)

To a solution of ZPF or M6 (1.3 mmol) in DMF, the corresponding 4-dimethylaminopyridine (DMAP) (3.9 mmol), N-hydroxysuccinimide (NHS) (2.6 mmol) and 1-ethyl-3-(3-dimethylaminopropyl) carbodiimide hydrochloride (EDC·HCl) (2.6 mmol) were added, and the mixture was stirred at 35 °C for 2 h; then, the 2-thiophenecarboxaldehyde hydrazone (1.5 mmol) was added to the reaction mixture. After the reaction was completed, the reaction mixture was poured into ice-water and the formed crude product was collected by filtration [26]. The target product was obtained by recrystallised from methanol.

2.2. Cell culture

The murine macrophage cell line RAW264.7, obtained from the American Type Culture Collection, was purchased from the China Center for Type Culture Collection. RAW264.7 cells were cultured in Dulbecco's modified eagle medium (DMEM) (Hyclone, USA), supplemented with with penicillin–streptomycin solution (Gibco, USA), L-Glutamine (Gibco, USA) and 10 % fetal bovine serum (PAN, Germany). The cultures were maintained at 37 °C in a humidified atmosphere containing 5 % CO_2. Twenty-four hours after seeding, the culture medium was replaced with a serum-free medium and the cells were incubated for 12 h before undergoing chemical treatment. For example, the cells were pre-incubated with GW9662 (2-chloro-5-nitrobenzanilide) (Beyotime, China) for 2 h or ZPF and its metabolites for 2 h, and 0.1 μg/mL LPS (Beyotime, China) for 22 h. All experiments were performed at least in triplicate on three separate occasions [27].

CHO (Chinese Hamster Ovary) cells were obtained from China Center for Type Culture Collection, Wuhan. CHO cells were cultured in DMEM/F-12 (Dulbecco's minimum essential medium/nutrient F-12) (Thermo Fisher Scientific, China) with penicillin–streptomycin solution (Gibco, USA), L-Glutamine (Gibco, USA) and 10 % fetal bovine serum (PAN, Germany) added [28]. The cultures were maintained at 37 °C in a humidified atmosphere containing 5 % CO_2. Moreover, the hamster ovary CHO cell transfection of the wild-type and mutant vectors of COX-2 was conducted by ExFect®2000 Transfection Reagent (Vazyme, China) according to the manufacturer's instructions.

2.3. Cell viability assay

Cell viability was determined using cell CCK-8 (counting kit-8) assay. RAW264.7 cells were seed into 96-well plates and cultured for 24 h, followed by incubation with varying concentrations of ZPF and its metabolites (5–160 μM) for 24 h. Subsequently, 10 μL of the CCK-8 solution (Vazyme, China) was added to each well of the plate, and the plate was incubated for 1–4 h in the 37 °C incubator (Thermo, USA). Absorbance was then measured at 450 nm using a microplate reader (EnVision, USA). Control cells were treated with CCK-8 solution, the absorbance of which was taken as 100 % viability.

2.4. In vitro cyclooxygenase inhibition assay

The inhibitory effects of ZPF and its metabolites on COX-1 and COX-2 were evaluated using the commercially available COX-1 (ovine) inhibitor screening assay kit (Biovision, USA) and COX-2 (human) inhibitor screening assay kit (Beyotime, China) [29]. The reaction steps are performed strictly following the manufacturer's instructions. Briefly, ZPF and its metabolites at final concentration of 10, 20, 40, 80, 160, 320, 640 and 1280 nM, were incubated with ovine COX-1, human recombinant COX-2 and arachidonic acid solution to initiate COX reaction. After incubation, prostaglandins were quantified by measuring fluorescence values using a microplate reader (Tecan Infinite Pro, Switzerland) at Ex/Em = 535/587 nm for COX-1 and Ex/Em = 560/590 nm for COX-2.

2.5. Molecular docking and PyMOL analysis

The crystal structure of human COX-2 proteins (PDB ID 5IKQ), COX-1 (PDB ID 5WBE), NALP3 PYD (PDB ID 3QF2), MD-2 (PDB ID 2E59), and PPAR-γ (PDB ID 4XTA) was obtained from the PDB database (https://www.rcsb.org/). Moreover, SYBYL-X 2.0 was utilized for the molecular docking between COX-2, COX-1 and PPAR-γ proteins and ZPF along with its metabolites, and the key amino acid (AA) residues involved in hydrogen bond formation between the proteins and compounds were identified. The specific parameter settings of the docking software: Docking mode is Surflex-Dock, protein molecules need to be removed from water molecules and added hydrogens, ligand molecules need to be added hydrogens and optimized. Furthermore, AA residues within 5Å of the active pocket were considered to be key AA residues that may be related to affinity. Furthermore, the docking results and the "STSBPT" were analysed and visualized using PyMOL software [30].

2.6. Establishment and evaluation of COX-2 activity model of CHO cells

The design and analysis of mutation sites depends on SIFT (https://sift.bii.a-star.edu.sg/) and PolyPhen-2 (https://genetics.bwh.harvard.edu/pph2/). SIFT utilizes the homology and physical properties of AA residues sequences to predict whether the substitution of AA residues will impact protein function, while also assessing the degree of harmfulness caused by gene variations [31]. PolyPhen-2 predicts the possible effects of AA residues substitution on the stability and function of human proteins in terms of structure and comparative evolution [32]. Generally, a lower SIFT score and a higher PolyPhen-2 score indicate a less favorable mutation with a more significant impact on protein function [33]. Following this principle and the docking results, key AA residues are mutated to disrupt protein function. Briefly, the lists of AA residues of the active pocket from docking results were predicted by SIFT software with the score of 0. These sites were taken into PolyPhen-2 to further select mutation sites with a score of 1.

Evaluation of COX-2 activity in a CHO cell model was modified in the present research study [34]. CHO cells transfected with wild-type and mutant vectors of COX-2 were digested with trypsin 0.25 % (w/v) (Hyclone, USA), and then collected by centrifugation at 1000 rpm for 5 min. CHO cells were washed with Hank's balanced salt solution (HBSS) buffer (Thermo Fisher, USA) once, and resuspended in HBSS buffer (2.0×10^5 cells/mL). CHO cells were seeded in 48-well plates at 500 μL per well (1.0×10^5 cells/well), and incubated with the test compound (final concentration 100 μM ZPF, M2, M3 and M5) or dimethyl sulfoxide (DMSO) (Solarbio, China) for 15 min at 37 °C before challenged with arachidonic acid. Cells were challenged for 15 min with an arachidonic acid solution (10 % ethanol in HBSS) to yield final concentrations of 10 μM arachidonic acid in the CHO [COX-2] assay. Positive control reactions (DMSO incubation, arachidonic acid and without test compound) and negative control reactions (DMSO incubation, without arachidonic acid and test compound) were set for each experiment. Then, 25 μL 1 M HCl was added to stop the reaction, followed by 50 μL 0.5 M NaOH for neutralisation. After centrifugation at 2500 rpm for 20 min, the supernatant was collected and prostaglandin E2 (PGE2) production was measured by Human PGE2 ELISA Kit (Bioswamp, China). IR %=(Cp-Ct)/(Cp-Cn) × 100 %, (IR: the inhibitor ratio of COX-2 enzyme activities; Cp: positive concentration; Cn: negative concentration; Ct: test concentration).

2.7. Quantitative real-time PCR analysis (RT-qPCR)

The mRNA levels of the selected genes were assessed using the Bio-Rad CFX 96^{TM} RT-qPCR (Hercules, CA). Briefly, RAW264.7 cells were seeded into 12-well cell culture plate and cultured at 37 °C in a 5 % CO_2 humidified atmosphere. The cells were then pre-treated with ZPF and its analogues for 2 h, followed by treatment with 0.1 μg/mL LPS for 22 h. Subsequently, the cells were washed with phosphate-buffered saline

Table 1
The list of primers sequences.

Genes name	Primer sequence (5′-3′)	
COX-2	forward	TCCCTGAAGCCGTACACATCA
	reverse	TGGACGAGGTTTTTCCACCA
PPAR-γ	forward	GACCTGAAGCTCCAAGAATACCAAA
	reverse	TGAGGCCTGTTGTAGAGCTGGGTC
i-NOS	forward	GAGCGAGGAGCAGGTGGAA
	reverse	CCATAGGAAAAGACTGCACCGA
GAPDH	forward	AACTTTGGCATTGTGGAAGG
	reverse	ACACATTGGGGGTAGGAACA

(PBS) (Servicebio, China). Total RNA was extracted using the RNA isolater Total RNA Extraction Reagent (Vazyme, China) according to the manufacturer's instructions. The final RNA concentration and purity was determined using a Q3000 ultra-micro spectrophotometer (Thermo Fisher, USA), obtaining A260/A280 ratios between 1.9 and 2.1 in all the samples. One microgram of total RNA was immediately reversed transcribed to cDNA by HiScript II 1st strand cDNA synthesis kit (+gDNA wiper) (Vazyme, China). The cDNA was amplified by RT-qPCR using a ChamQ SYBR Color qPCR Master Mix (Vazyme, China) according to the manufacturer's instructions. Data from the reaction were collected and analysed by complementary computer software. Relative quantification of gene expression was calculated using the $2^{-\triangle\triangle Ct}$ method, and normalised to GAPDH in each sample. All of the primers used in this research study are shown in Table 1.

2.8. Western blot

After the treatment, RAW264.7 cells were collected, and total proteins were extracted using RIPA solution (Servicebio, China) supplemented with a protease and phosphatase inhibitor mixture (Beyotime, China). Cytosolic and nuclear proteins from cells were isolated using a cytosolic and nuclear extraction kit (Beyotime, China). Protein concentrations were determined with the enhanced BCA (bicinchoninic acid) protein assay kit (Beyotime, China) according to the manufacturer's instructions. Subsequently, 20 μg of cellular protein from each group were separated via 10 % SDS-PAGE (Sangon Biotech, China) and transferred onto PVDF (polyvinylidene difluoride) membrane (Millipore, USA). Membranes were blocked with 5 % BSA (bovine serum albumin) in 0.1 % Tween 20/Tris-buffered saline (TBST) (Servicebio, China) at room temperature for 1 h and then incubated overnight at 4 °C with COX-2, PPAR-γ, i-NOS, IL-1β, TNF-α, p-NF-κB p65, NF-κB p65, p-IκBα, IκBα, H3, and GAPDH antibody (Abclonal, China), or p-ERK, ERK, p38, p-p38, JNK, p-JNK antibody (CST, USA). After incubation, the membranes were washed three times with 0.1 % TBST and then incubated with secondary antibodies (1:5000 dilution) (Abclonal, China) at room temperature for 1.5 h. The enhanced chemiluminescence kit (Abclonal, China) was used to visualise the protein bands.

2.9. Immunofluorescence

Murine RAW264.7 cells were pretreated with ZPF and its analogues for 2 h, followed by stimulation with LPS for an additional 22 h. Subsequently, the cells were washed twice with TBS and fixed in 4 % paraformaldehyde (Servicebio, China) and permeabilised in TBS containing 0.3 % Triton X-100 (Solarbio, China) for 10 min. After blocking with 5 % BSA at 37 °C for 30 min, the samples were incubated overnight at 4 °C with primary antibodies, rabbit anti-NF-κB p65 and PPAR-γ (1:200, Abclonal, China). The samples were kept at room temperature and reheated for 15 min, followed by incubation with Cy3 Goat Anti-Rabbit IgG (H + L) (1: 200, Abclonal, China) as the secondary antibody. After being incubated in DAPI staining working solution (Servicebio, China) at room temperature for 10 min, the DAPI staining working solution was removed, and a drop of anti-fluorescence attenuation sealant (Servicebio, China) was applied to seal the coverslip. Imaging was conducted using laser scanning confocal microscopy (LSM 800, Zeiss, Germany), and data analysis was performed with ZEN software.

2.10. Cellular thermal shift assay and drug affinity responsive target stability

Engagement between ZPF/M2 and COX-2/PPAR-γ in RAW264.7 cells was analysed by cellular thermal shift assay (CETSA). Samples were prepared from DMSO-exposed cells and ZPF/M2-exposed cells. For each set, 2×10^7 cells were seeded in a 10-cm culture dish. RAW264.7 cells were treated with 0.1 μg/mL LPS for induction. After 24 h of culturing, the cells were washed with ice-PBS, scraped and collected. The samples were centrifuged at 12,000 rpm for 2 min at room temperature, and the pellets were gently resuspended with 0.5 mL of PBS containing 1 % protease inhibitors and 1 % phosphatase inhibitors (Beyotime, China). Then, the samples underwent three freeze–thaw cycles. For each cycle, they were exposed to liquid nitrogen for 3 min, placed in a heating block at 25 °C for 3 min. The samples were then centrifuged at 12,000 rpm for 10 min at 4 °C, and equal volume of supernatant was transferred to two new Eppendorf (EP) tubes, the DMSO group and the ZPF/M2 group. For the experimental sample set, ZPF/M2 was added to a final concentration of 100 μM and for the control sample set, the same volume of DMSO was added. The samples were incubated at 25 °C for 30 min and dispensed into 100 μL aliquots. Pairs consisting of one control aliquot and one experimental aliquot were heated at 41 °C, 45 °C, 49 °C, 53 °C, 57 °C, 61 °C for 3 min, and then placed at room temperature for 3 min. Lastly, the samples were placed on ice and subjected to Western blot analysis using primary antibody rabbit COX-2 or PPAR-γ (Abclonal, China).

Engagement between ZPF/M2 and COX-2/PPAR-γ in RAW264.7 cells was also analysed by DARTS [35]. Briefly, samples were prepared from cells exposed to DMSO and ZPF/M2. For each set, 2×10^7 cells were seeded in a 10-cm cultured dish. RAW264.7 cells were treated with 0.1 μg/mL LPS for induction. After 24 h of culturing, the cells were washed with ice-cold PBS, scraped and collected. The samples were centrifuged at 12,000 rpm for 2 min at 4 °C, and then the pellets were gently resuspended with 1.6 mL of M−PER (Thermo Scientific, USA) containing 1 % protease inhibitors and 1 % phosphatase inhibitors (Beyotime, China) and placed on ice for 20 min. The samples were centrifuged at 13,000 rpm for 3 min at 4 °C. The supernatant (cell lysate) was removed and transferred to a new 1.5 mL tube and keep on ice, and then add appropriate volume of 10 × TNC buffer [500 mM Tris-HCl (pH = 8.0), 500 mM NaCl, 100 mM $CaCl_2$] was added to make a final concentration of 1 × TNC buffer in the lysate. The protein concentration of cell lysate was determined by BCA protein concentration assay, and the protein concentration was adjusted to 6 g/L with precooled PBS buffer. The supernatant protein was divided into two EP tubes of equal volumes, and equal volumes of DMSO and ZPF/M2 were added, making a final concentration of ZPF/M2 for 100 μM; the two EP tubes were placed together on a shaker (Kylin-bell, China) at room temperature for shaking (10 rpm) and incubation (30 min). The protease was diluted in 1 × TNC buffer to a range of protease solutions. After incubation with the small molecule was complete, each sample was split into 100 μL aliquots, with 2 μL of the range of protease solutions, and the concentration of protease was made up to 1:100, 1:300, 1:1000, 1:3000 and 1:10000; the solutions were incubated for 30 min at room temperature. Each digestion reaction was stopped by adding 2 μL of 100 × protease inhibitor cocktail (Thermo Fisher, USA) and then incubated on ice for 10 min. Next, 5 × SDS-PAGE loading buffer (Beyotime, China) was added to the samples to achieve a final concentration of 1 × SDS-PAGE loading buffer. The solution was finally heated at 95 °C for 10 min, and subjected to Western blot analysis using primary antibody rabbit COX-2 or PPAR-γ (Abclonal, China).

2.11. Model of LPS-induced acute lung inflammation and grouping

The specific pathogen-free (SPF) male C57BL/6 mice, aged 6–8

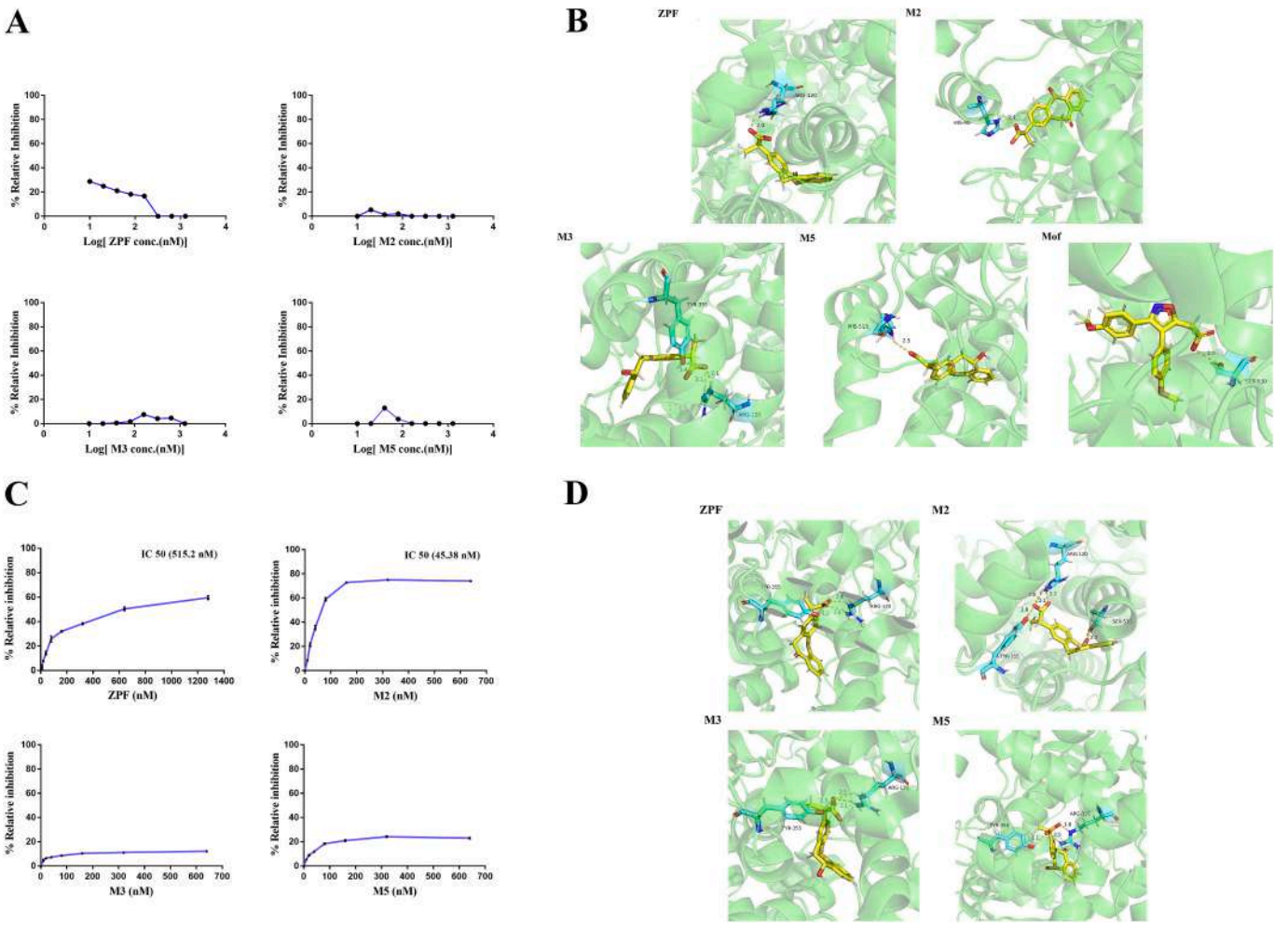

Fig. 4. The inhibitory effect of ZPF and its metabolites on the COX enzyme. Inhibitory effect and binding properties of ZPF and its metabolites on the COX-1 enzyme (A, B). Inhibitory effect and binding properties of ZPF and its metabolites on the COX-2 enzyme (C, D).

weeks and weighing 18–22 g, were obtained from the Centre of Laboratory Animals of Huazhong Agricultural University. The research protocol was approved by the Animal Ethics Committee of the Faculty of Veterinary Medicine (Huazhong Agricultural University, Wuhan, P.R. China). Animals were housed in well-maintained rooms at a temperature of 20–26 °C, with a relative humidity of 40–70 % and a 12 h light/dark cycle. During the first week of acclimatization, all animals received basic feed and fresh water.

For the ZPF and M2 treatments, ZPF and its metabolite M2 were dissolved in DMSO and subsequently diluted in PBS. Mice were randomly divided into six groups (n = 8 per group): a control group received PBS-DMSO, a group receiving LPS only, a group receiving ZPF without LPS, a group receiving the metabolite M2 without LPS, an experimental group receiving ZPF followed by LPS, and an experimental group receiving metabolite M2 followed by LPS. The mice were sacrificed by intraperitoneal injections of sodium pentobarbital (100 mg/kg b.w.) after intraperitoneal injection of ZPF/M2 (30 mg/kg b.w.) for 2 h and intraperitoneal injection of LPS (10 mg/kg b.w.) for 6 h. For analogue treatment, analogues were dissolved in DMSO and diluted in PBS. Mice were randomly divided into twelve groups (n = 8 per group): a control group which received PBS-DMSO, a group receiving LPS only, five groups receiving different analogues (D63, E63, JMC2, JMC5 and JMC6, which may have a stronger anti-inflammatory effect, were obtained by using the principle of chemical splicing without LPS, and five experimental groups receiving different analogues (D63, E63, JMC2, JMC5 and JMC6) followed by LPS [36,37]. The mice were sacrificed after intraperitoneal injection of analogues (30 mg/kg b.w.) for 2 h and intraperitoneal injection of LPS (10 mg/kg b.w.) for 6 h [38]. Then, the left lung was collected to obtain the "wet" weight, and then left lung was dried in an oven at 80 °C for 72 h and weighed to obtain the "dry" weight. Lung edema was assessed by calculating lung wet/dry (W/D) ratio. Meanwhile, the right lung tissues were collected for pathological examination and histochemical analysis.

2.12. Histopathological analysis and immunohistochemical staining (IHC)

All histopathological assays were performed using standard laboratory procedures. The upper lobe of the right lung of each male C57BL/6 mice (6–8 weeks old) was fixed in 4 % buffered paraformaldehyde, dehydrated using a gradient series of alcohol, embedded in paraffin, and sliced into 5 μm sections. The prepared slides were stained with hematoxylin-eosin (HE) staining (Baiqiandu, China), and examined under an optical microscope (NIKON Eclipse ci, Japan) to observe morphological changes. Immunohistochemical staining was carried out to assess protein expression levels of COX-2 and PPAR-γ. Primary antibodies of COX-2 and PPAR-γ (Abclonal, China) were incubated overnight at 4 °C. For immunohistochemical analysis, secondary antibodies of Abclonal goat anti-rabbit IgG were incubated for 50 min at room temperature. The sections were then mounted and examined under a Nikon Eclipse E100 optical microscope.

Table 2
Results of chemicals docking with 5WBE. The binding of the chemicals to COX-1 (PDB ID 5WBE) was analysed by SYBYL-X 2.0 and PyMOL software.

Chemicals	COX-1 PDB ID	Key residues	Docking scores
ZPF	5WBE	Arg120	5.2061
M2	5WBE	His90	3.9232
D63	5WBE	Arg120	6.6408
E63	5WBE	Arg120 Ser530	4.3308
JMC2	5WBE	Arg120 Tyr385	0.3378
JMC5	5WBE	Tyr385 Ser530	1.2914
JMC6	5WBE	Arg120	6.4197
Mofezolac	5WBE	Ser530	8.3543

Table 3
Results of chemicals docking with 5IKQ. The binding of the chemicals to COX-2 (PDB ID 5IKQ) was analysed by SYBYL-X 2.0 and PyMOL software.

Chemicals	COX-2 PDB ID	Key residues	Docking scores
ZPF	5IKQ	Arg120 Tyr355	8.3609
M2	5IKQ	Arg120 Tyr355 Ser530	8.4923
D63	5IKQ	Arg120	9.2240
E63	5IKQ	Arg120 Ser530	9.0971
JMC2	5IKQ	Tyr115 Arg120 Ser530	8.5525
JMC5	5IKQ	Arg120	6.3808
JMC6	5IKQ	Arg120 Tyr355 Arg513 Ser530	9.4747

2.13. Data and statistical analysis

Statistical analysis was performed using SPSS 18.0 for Windows. All of the results were presented as the mean ± standard deviation. Differences between multiple groups were analyzed using a one-way analysis of variance. Statistical significance was set at $p < 0.05$ and a value of $p < 0.01$ was strongly significant.

3. Results

3.1. Zaltoprofen (ZPF) and metabolite M2 have COX-2 inhibitory activity but not COX-1 inhibitory activity

The COX-1 and COX-2 inhibitory activities of ZPF and its main metabolites were evaluated using the COX-1 (ovine) and COX-2 (human) inhibitor screening assay kit. It can be seen from Fig. 4A that the relative inhibition rate of ZPF and its metabolites on COX-1 was less than 50 %, in the order ZPF, M5, M3 and M2 (from high to low). Further analysis by molecular docking using mofezolac (Mof, a NSAID and selective COX-1 inhibitor) as the positive binding ligand of COX-1, showed that the docking score of ZPF and its metabolites with COX-1 was much lower than that of mofezolac. The binding of key AA residues was completely different to mofezolac (Fig. 4B and Table 2), further indicating that ZPF and its metabolites did not have inhibitory activity against the COX-1 enzyme. In addition, as can be seen from Fig. 4C, the IC_{50} values of metabolite M2 and ZPF were 45.38 nM and 515.2 nM, respectively, indicating that metabolite M2 has a better inhibitory activity on COX-2 than ZPF, while metabolite M3 and metabolite M5 had almost no inhibitory effect on COX-2. The inhibition of COX-2 activity by ZPF and its metabolites was further confirmed by the molecular docking assay, where the docking score for metabolite M2 was higher than ZPF and its other metabolites (Fig. 4D and Table 3). The above results show that the inhibitory activity of metabolite M2 on the COX-2 enzyme was greater than the other compounds, while the inhibitory activity of metabolite M2 on the COX-1 enzyme was less than the other compounds.

3.2. PPAR-γ was predicted as an anti-inflammatory molecular signalling target based on STSBPT

To investigate the multiple pharmacodynamic molecular signalling

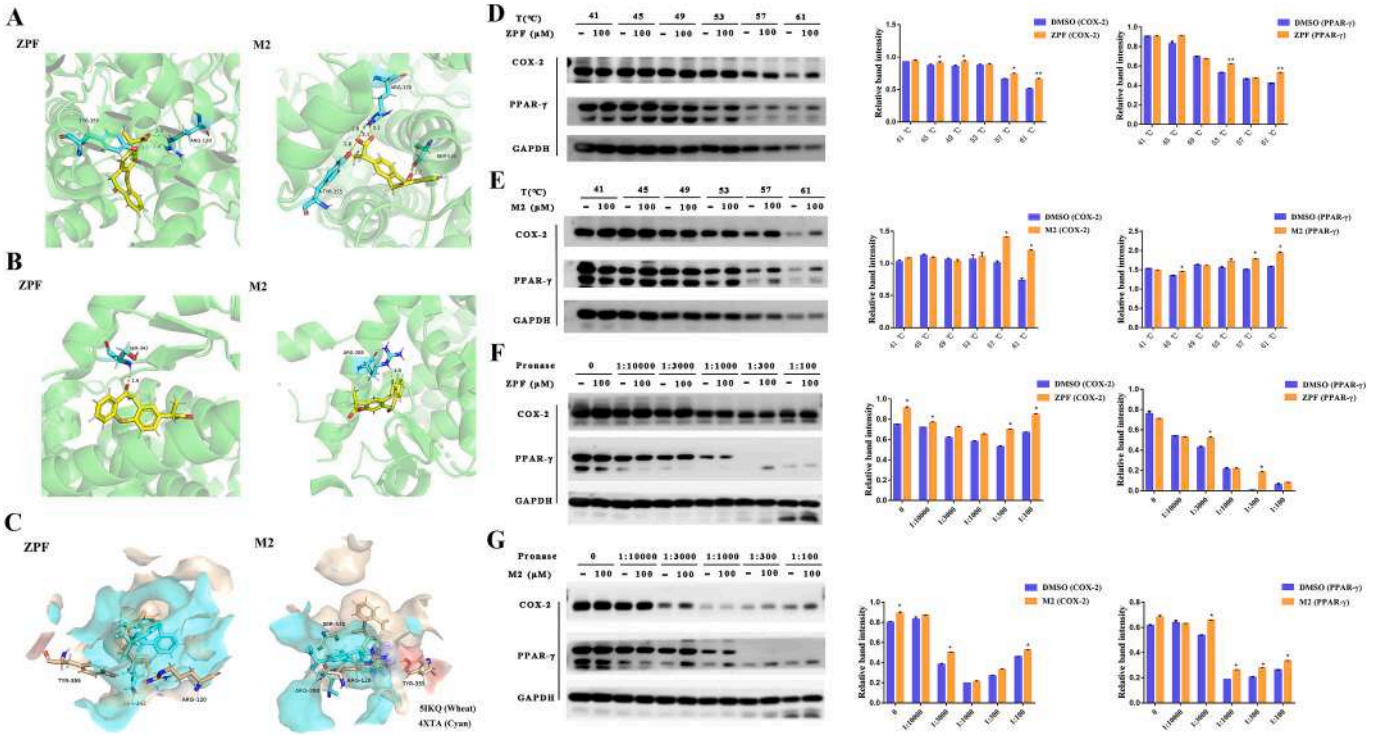

Fig. 5. Prediction of PPAR-γ as an anti-inflammatory molecular target based on the STSBPT strategy. The binding of ZPF and its metabolite M2 with COX-2 and PPAR-γ was simulated by molecular docking (A, B). The degree of similarity of the COX-2 and PPAR-γ pocket was simulated based on the STSBPT strategy (C). The binding potential of ZPF and M2 with COX-2 and PPAR-γ was analysed by CETSA (D, E). The binding potential of ZPF and M2 with COX-2 and PPAR-γ was analysed by DARTS (F, G). Statistical analysis was conducted by one-way ANOVA followed by Bonferroni's for multiple comparisons. All experiments were repeated in triplicate and data were represented as the mean ± SD from a represent experiments (n = 3). *$p < 0.05$, **$p < 0.01$ *vs.* DMSO (COX-2) group or DMSO (PPAR-γ) group.

Table 4
Results of chemicals docking with 4XTA. The binding of the chemicals to PPAR-γ (PDB ID 4XTA) was analysed by SYBYL-X 2.0 and PyMOL software.

Chemicals	PPAR-γ PDB ID	Key residues	Docking scores
ZPF	4XTA	Ser342	3.3534
M2	4XTA	Arg288	5.3303
D63	4XTA	Arg288 Ser342 Glu343	7.2936
E63	4XTA	Arg288	6.7424
JMC2	4XTA	Arg288 Ser342	8.8142
JMC5	4XTA	Arg288 Ser342 Leu288	9.4084
JMC6	4XTA	Arg288 Glu295	8.2928

targets of ZPF and its metabolite M2, the STSBPT strategy was employed to predict the topological structure-like spatial binding properties of proteins associated with inflammation regulation, including PPAR-γ, NLRP3 and TLR4-MD2. SYBYL-X 2.0 software was utilized to analyse the key AA residues of ZPF and metabolite M2 binding to the PPAR-γ crystal (PDB:4XTA) and the COX-2 crystal (PDB:5IKQ) with known NSAID compounds as ligands. The results showed that arginine 120 (Arg120) and tyrosine 355 (Tyr355) are the key AA residues for ZPF binding to COX-2, while Arg120, Tyr355 and serine 530 (Ser530) are the key AA residues for M2 binding to COX-2 (Fig. 5A). Meanwhile, the key AA residues of ZPF and metabolite M2 binding to PPAR-γ were Ser342 and Arg288, respectively (Fig. 5B and Table 4). It is worth noting that, as shown in Fig. 5, both ZPF and metabolite M2 have binding characteristics with PPAR-γ and COX-2, and their binding characteristics have a similar spatial structure. In order to further verify the similarity in spatial structure of the binding pockets, PyMOL, a cross-platform molecular graphics tool, was used to analyse the spatial similarity of the binding pockets of ZPF/M2 and COX-2/PPAR-γ. As shown in Fig. 5C, the binding activity pockets of ZPF/M2 and COX-2/PPAR-γ have a high degree of structural similarity in space. In addition, the spatial similarity of the binding pockets of ZPF/M2 and COX-2/NLRP3/MD2 was also analysed by SYBYL-X 2.0 software and PyMOL, which showed that the ZPF/M2-NLRP3/MD2 binding active pockets had poor spatial similarity with the ZPF/M2-COX-2 binding active pockets. In addition, CETSA and DARTS were used to analyse the potential of ZPF/M2 binding to COX-2/PPAR-γ. As shown in Fig. 5D-G, the results indicate that the COX-2 and PPAR-γ proteins in the ZPF/M2 group had better thermal stability and enzyme stability compared to the DMSO group. The above results suggest that COX-2/PPAR-γ might be a potential anti-inflammation target of ZPF/M2.

3.3. ZPF/M2 suppressed NF-κB and reversed PPAR-γ activity in LPS-stimulated RAW264.7 cells

The results of the anti-inflammatory activity of ZPF and its metabolite M2 in LPS-stimulated RAW264.7 cells showed that both ZPF and M2 have significant anti-inflammatory effects, and the anti-inflammatory effect of M2 on the expression of COX-2, i-NOS and PPAR-γ is significantly stronger than ZPF (Fig. 6A, B). To further investigate whether the PPAR-γ/NF-κB molecular signalling pathway could be regulated by ZPF and metabolite M2, the nuclear transfer related proteins, p-p65 and p-IκBα, were detected in RAW264.7 cells. As shown in Fig. 6C, D, compared to the control group, LPS could significantly increase the p-IκBα gene and PPAR-γ levels and decrease the p-p65 level in the cytoplasm. However, ZPF and metabolite M2 significantly reversed the LPS-induced p-IκBα and PPAR-γ levels and further decreased the transcription factor NF-κB/p-p65 level in the cytoplasm. Meanwhile, ZPF and metabolite M2 significantly decreased the accumulation of p-p65 and increased the PPAR-γ levels in the nucleus, especially at 160 μM. The nuclear localisation of NF-κB and PPAR-γ in RAW264.7 cells was further determined by immunofluorescence assay. The results of this study showed that LPS treatment significantly

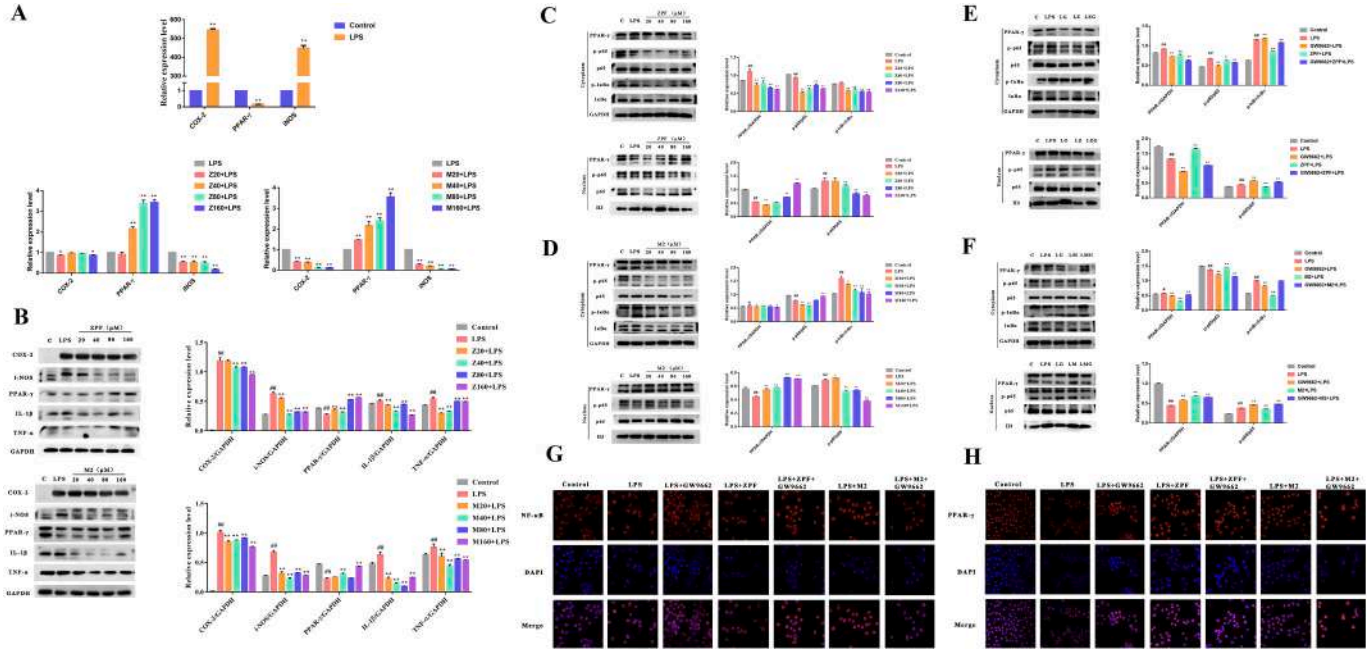

Fig. 6. Regulation of ZPF and its metabolite M2 on LPS-induced PPAR-γ inhibition and phosphorylated p65 activation. ZPF can inhibit the expression of COX-2 (to a certain extent), inhibit the expression of i-NOS and increase the expression of PPAR-γ induced by LPS in a concentration-dependent manner. Metabolite M2 can significantly inhibit LPS-induced COX-2 and i-NOS, and elevate PPAR-γ gene expression in a concentration-dependent manner, and the inhibitory effect is stronger than that of ZPF (A). ZPF and its metabolite M2 inhibit the inflammatory associated proteins induced by LPS, consistent with the trend of mRNA (B). ZPF and its metabolite M2 can inhibit phosphorylated p65 and activate PPAR-γ in a concentration-dependent manner (C, D). The presence of GW9662 can block the regulation of ZPF and its metabolite M2 on phosphorylated p65 and PPAR-γ (E, F). The effects of ZPF and its metabolite M2 on the nuclear transfer of p65 and PPAR-γ were detected by immunofluorescence assay (G, H). Statistical analysis was conducted by one-way ANOVA followed by Bonferroni's for multiple comparisons. All experiments were repeated in triplicate and data were represented as the mean ± SD from a represent experiments (n = 3). $^{**}p < 0.01$ *vs.* control group; $^{*}p < 0.05$, $^{**}p < 0.01$ *vs.* LPS group + different conditions group; $^{\#}p < 0.05$, $^{\#\#}p < 0.01$ *vs.* control group and LPS group.

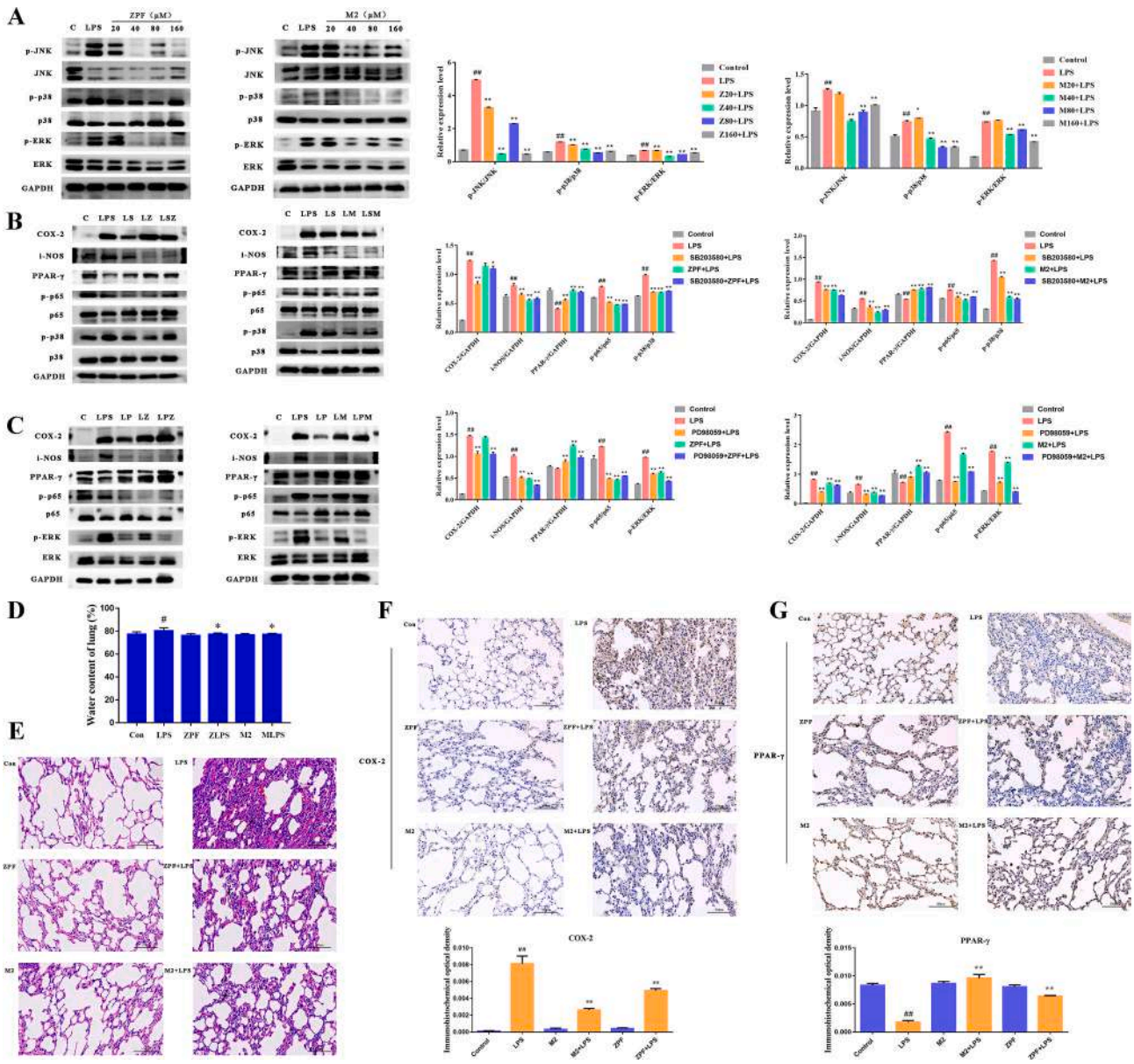

Fig. 7. ZPF and its metabolite M2 regulate the expression of PPAR-γ and p65 through the MAPK signalling pathway in RAW264.7 cells and LPS-induced ALI in mice. ZPF and its metabolite M2 can significantly inhibit p-JNK, p-ERK and p-p38 expression in a concentration-dependent manner (A). The presence of p38 inhibitors (SB203580) or ERK1/2 phosphorylation inhibitor (PD98059) can significantly reduce the expression of COX-2, i-NOS and p-p38, and improve the expression level of PPAR-γ; ZPF and its metabolite M2 can significantly inhibit LPS-induced pulmonary oedema in mice (B, C). ZPF and M2 could significantly reverse the water content of the lung induced by LPS (D). The inhibitory effect of ZPF and its metabolite M2 on LPS-induced lung injury in mice was observed by histopathology (E). The changes of COX-2 and PPAR-γ in the lung tissues of mice were analysed by immunohistochemistry (F, G). Statistical analysis was conducted by one-way ANOVA followed by Bonferroni's for multiple comparisons. All experiments were repeated in triplicate and data were represented as the mean ± SD from a represent experiments (n = 3). $^{\#}p < 0.05$, $^{\#\#}p < 0.01$ *vs* control group and LPS group; $^{*}p < 0.05$, $^{**}p < 0.01$ *vs* LPS group + different conditions group.

promoted the transfer of NF-κB and inhibited the transfer of PPAR-γ from the cytoplasm to the nucleus. However, NF-κB and PPAR-γ were mainly concentrated in the cytoplasm and nucleus, respectively, after pre-treatment with ZPF and M2 (Fig. 6G, H), which means that ZPF and M2 inhibit LPS-induced NF-κB nuclear transfer in RAW264.7 macrophage cells but promote the nuclear transfer of PPAR-γ. In addition, the presence of GW9662, a PPAR-γ antagonist, can reverse the effects of ZPF and M2 to a certain extent (Fig. 6E-H). The above research shows that PPAR-γ can regulate NF-κB levels. Taken together, the activation of nuclear factor NF-κB and the inhibition of PPAR-γ induced by LPS was suppressed by ZPF and metabolite M2, suggesting that ZPF and M2 have anti-inflammatory effects through the PPAR-γ/NF-κB signalling pathway.

3.4. ZPF/M2 alleviated the MAPK-PPAR-γ/NF-κB signalling pathways induced by LPS in RAW264.7 cells

The MAPK (mitogen-activated protein kinase) pathways play a critical role in various cellular processes, including proliferation, differentiation, apoptosis, cell survival, cell motility, metabolism, stress response and inflammation. These pathways are also thought to regulate the PPAR-γ and NF-κB signalling pathways [39,40]. Therefore, the present research study investigated whether ZPF/M2 could be involved in the regulation of MAPKs signaling pathway.

As shown in Fig. 7A, ZPF and M2 significantly reduced the phosphorylation levels of JNK (c-Jun N-terminal protein kinase), ERK1/2 (extracellular signal-regulated kinase 1/2) and p38 MAPK (mitogen-

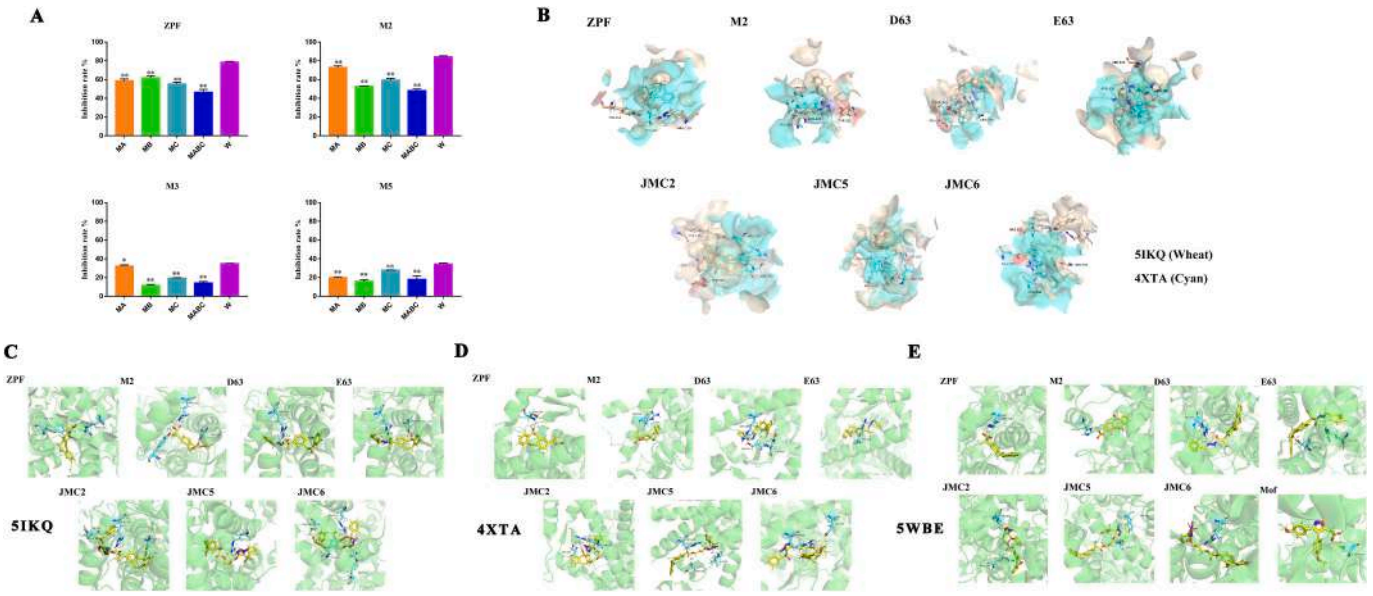

Fig. 8. Novel analogues of ZPF and its metabolite M2 were designed based on the COX-2 active site and the STSBPT strategy. The key AA residues inhibited by ZPF and its metabolite M2 on COX-2 were analysed by the Chinese hamster ovary (CHO) model. MA, MB, MC, MABC and W represent COX-2 with an Arg120 site mutation, a Tyr355 site mutation, a Ser530 site mutation, a triple point combination of Arg120, Tyr355, and Ser530, and wild-type COX-2, respectively (A). Based on the STSBPT strategy, the high similarity of the binding pockets and key amino acids of the novel analogues with COX-2 and PPAR-γ were analysed (B, C, D). The binding potential of the novel analogues with COX-1 was predicted (E). Statistical analysis was conducted by one-way ANOVA followed by Bonferroni's for multiple comparisons. All experiments were repeated in triplicate and data were represented as the mean ± SD from a represent experiments (n = 3). $^{*}p < 0.05$, $^{**}p < 0.01$ *vs.* W group.

activated protein kinase p38) induced by LPS. Further research showed that M2 exhibited a significantly stronger inhibitory effect on the p38 signaling pathway compared to ZPF, whereas ZPF demonstrated a more pronounced inhibitory effect on the central ERK1/2 signaling pathway than M2.

Hence, in order to further explore whether the MAPK signalling pathway is interrelated with PPAR-γ/NF-κB and thus participates in the anti-inflammatory effects of ZPF and metabolite M2, a selective p38 MAPK inhibitor (SB203580) and MAPK (ERK1/2) phosphorylation inhibitor (PD98059) were used to treat an LPS-induced RAW264.7 murine macrophage cell line. As shown in Fig. 7B, the presence of the p38 MAPK inhibitor (SB203580) significantly reduced the protein expression levels of COX-2, i-NOS, p-p65, and p-p38 transcription complex in RAW264.7 murine macrophage cell-based assays induced by LPS, and increased the protein expression level of PPAR-γ. It is worth noting that ZPF, metabolite M2 and the p38 MAPK inhibitor (SB203580) basically show the same trend, and the inhibitory effect of M2 on p-p38, COX-2 and the activation of PPAR-γ is stronger than that of ZPF. Additionally, the presence of the ERK1/2 phosphorylation inhibitor (PD98059) significantly reduced the protein expression levels of COX-2, i-NOS, p-p65 protein and p-ERK protein in the LPS-induced RAW264.7 macrophage cell line, and increased the protein expression level of PPAR-γ. ZPF and metabolite M2 basically showed the same trend as the ERK1/2 inhibitor (PD98059), and the inhibitory effect of ZPF on the p-ERK signalling pathway was stronger than that of M2 (Fig. 7C). These results indicate that both ZPF and metabolite M2 can participate in the expression of COX-2 and i-NOS through the MAPK-PPAR-γ/NF-κB signalling pathways; meanwhile, ZPF and M2 focus on the regulation of the ERK and p38 MAPK activated protein kinases, respectively, thus playing a role in resisting the inflammatory response of the RAW264.7 macrophage cell line induced by LPS.

3.5. Verification of the in vivo activity of ZPF/M2 in LPS-induced acute lung injury (ALI) in mice

To further understand the role of ZPF and metabolite M2 in LPS-induced inflammation *in vivo*, the anti-inflammatory effect of intraperitoneal injection ZPF (30 mg/kg b.w.) and M2 (30 mg/kg b.w.) for 2 h, was investigated in the LPS (intraperitoneal injection 10 mg/kg b.w. for 6 h)-induced ALI in male C57BL/6 mice. Compared with the control group, the LPS group significantly increased the water content of the lung. However, the ZPF and M2 groups could significantly reverse the water content of the lung (Fig. 7D), indicating that ZPF and M2 have therapeutic effects on lung injuries induced by LPS. Further histopathological image analysis of the lung tissue showed that the lung tissue structure of the LPS group was abnormal compared to the control group, with a large amount of alveolar atrophy and collapse, alveolar wall thickening, lung parenchyma and surrounding alveolar fusion and expansion, as shown by the red arrow (Fig. 7E), and a large number of neutrophil infiltrations in the lung tissue, as shown by the black arrow (Fig. 7E). This means that the lung tissue of the LPS group showed a high degree of inflammatory cell infiltration. Meanwhile, the lung tissue structure of the ZPF and M2 treatment groups showed a significant relief effect compared to the LPS group, mainly reflected in the mild abnormality of the lung tissue, the thickening of some alveolar walls, and a small amount of neutrophil infiltration, as shown by the black arrow (Fig. 7E).

The COX-2 and PPAR-γ levels in the lung tissues were also detected by immunohistochemistry staining. The results showed that LPS can significantly increase COX-2 gene expression and decrease the expression of PPAR-γ, and that ZPF and M2 can attenuate the effects of LPS to some extent (Fig. 7F, G); a similar trend was also observed with chemiluminescent Western blotting. The above results indicate that ZPF and metabolite M2 can alleviate LPS-induced ALI in male C57BL/6 mice in a COX-2- and PPAR-γ-dependent manner.

3.6. Designing novel analogues (D63, E63, JMC2, JMC5 and JMC6) based on the STSBPT strategy

In order to identify more effective anti-inflammatory compounds, the key active residues of COX-2 were further verified by CHO (Chinese Hamster Ovary) cells. The findings of this study showed that Arg120,

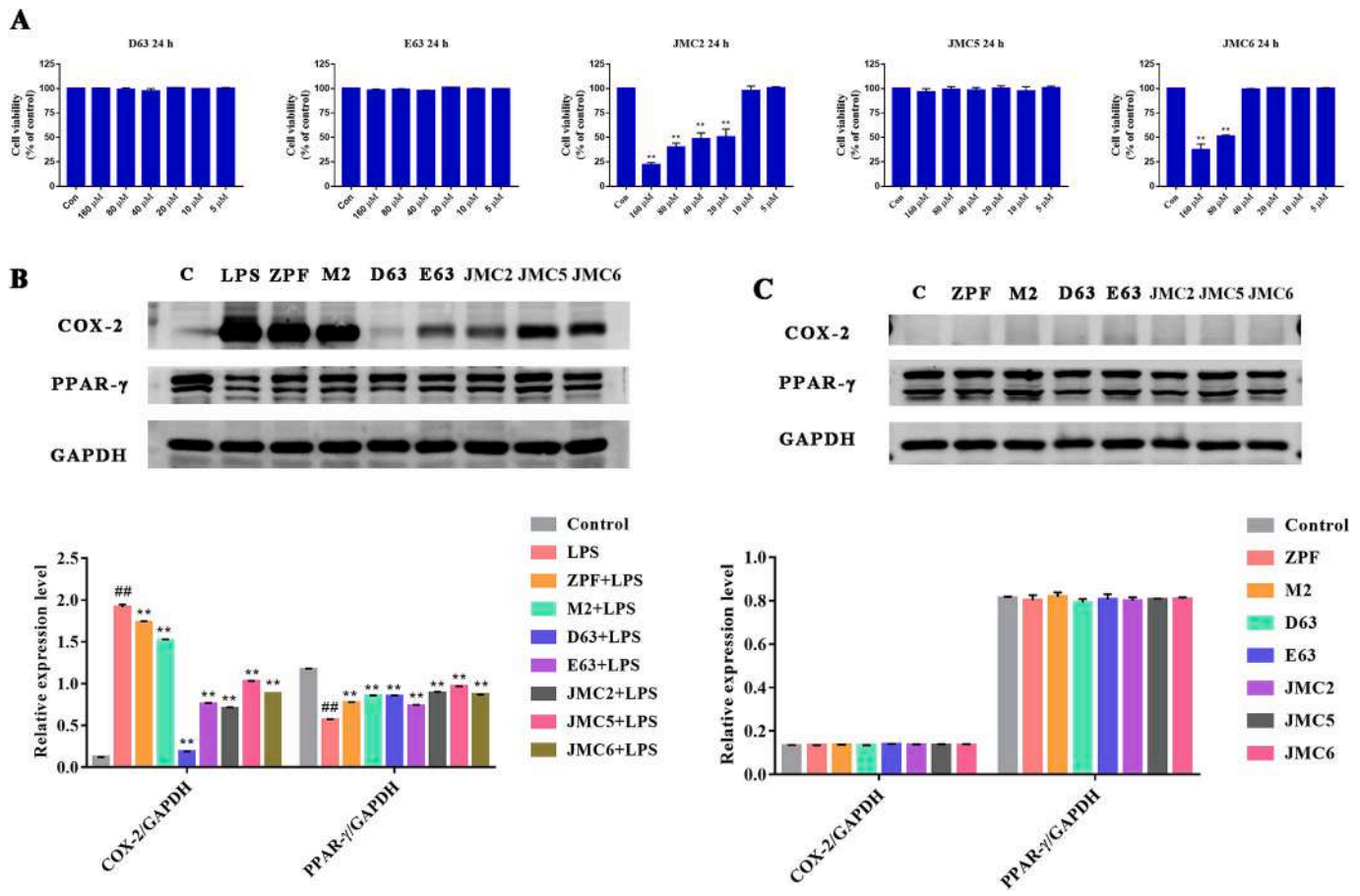

Fig. 9. Novel analogues: cytotoxicity and regulation of COX-2 and PPAR-γ. The cytotoxicity of novel analogues to RAW264.7 cells (A). Novel analogues can mitigate the effect of LPS on the elevation of COX-2 and the inhibition of PPAR-γ, and do not affect the expression of COX-2 and PPAR-γ themselves (B, C). Statistical analysis was conducted by one-way ANOVA followed by Bonferroni's for multiple comparisons. All experiments were repeated in triplicate and data were represented as the mean ± SD from a represent experiments (n = 3). $^{**}p < 0.01$ *vs.* control group $^{\#\#}p < 0.01$ *vs.* control group and LPS group; $^{**}p < 0.01$ *vs.* LPS group + different conditions group;

Tyr355 and Ser530 are the key active sites of COX-2 (Fig. 8A). Based on these key active sites, the docking scoring and the STSBPT, a series of compounds (D63, E63, JMC2, JMC5 and JMC6) were designed and synthesised using a parallel method. The STSBPT analysis showed that the novel analogues were highly similar to the COX-2 and PPAR-γ binding pockets, which means that the novel analogues have the dual target effect of COX-2 and PPAR-γ (Fig. 8B). Moreover, the key amino acids binding to COX-2 were Arg120, Tyr355 and Ser530 (Fig. 8C and Table 3), while the key amino acids binding to PPAR-γ were Arg288, Ser342 and Leu288 (Fig. 8D and Table 4). Analysis of the binding ability of the novel analogues to COX-1 showed that the key amino acid binding between the novel analogues and COX-1 was different to that of mofezolac; the docking score of the novel analogues to COX-1 was also lower than that of mofezolac to COX-1, indicating that the novel analogues did not possess COX-1 binding potential (Fig. 8E and Table 2). The above results demonstrate that the novel analogues have the dual targeting effects of COX-2 and PPAR-γ, but do not have COX-1 inhibitory activity.

3.7. Novel analogues (D63, E63, JMC2, JMC5 and JMC6) can mitigate LPS-induced changes in COX-2 and PPAR-γ levels

In order to further verify the dual target effect of the novel analogues on the inhibition of LPS-induced inflammation, the CCK-8 assay was used in this research study to evaluate the cytotoxicity of the novel analogues. The results of this research study showed that D63, E63, and JMC5 did not exhibit significant cytotoxicity, while JMC2 and JMC6 did not exhibit cytotoxic effects when the values were less than 10 μM and 40 μM, respectively. Therefore, in the subsequent experiments, the concentrations of the novel analogues D63, E63 and JMC5 was 160 μM, while those of JMC2 and JMC6 were 10 μM and 40 μM, respectively (Fig. 9A). Additionally, as shown in Fig. 9B, the novel analogues all had different degrees of resistance to the LPS-induced COX-2 expression in the RAW264.7 macrophages cell line, and the inhibitory effect was significantly stronger than that of ZPF and metabolite M2. Meanwhile, the novel analogues could alleviate the decrease of PPAR-γ protein levels in RAW264.7 macrophage cells induced by LPS. Interestingly, in the absence of LPS, the novel analogues did not significantly increase the protein expression levels of COX-2 and PPAR-γ (Fig. 9C), suggesting that the regulatory effect of the novel analogues on PPAR-γ may be dependent on the presence of COX-2. The above results indicate that the novel analogues have the ability to alleviate changes in COX-2 and PPAR-γ levels induced by LPS.

3.8. Verification of the in vivo activity of novel analogues (D63, E63, JMC2, JMC5 and JMC6) in LPS-induced ALI in mice

To further understand the role of the novel analogues in LPS-induced inflammation *in vivo*, the anti-inflammation effects of these novel analogues (D63, E63, JMC2, JMC5 and JMC6, intraperitoneal injection of 30 mg/kg b.w. for 2 h) were investigated in the LPS-induced ALI of male C57BL/6 mice. Compared with the control group, the LPS group (intraperitoneal injection 10 mg/kg b.w. for 6 h) significantly increased the water content of the lung. However, all of the novel analogues could significantly reverse the water content of the lung (Fig. 10A), indicating

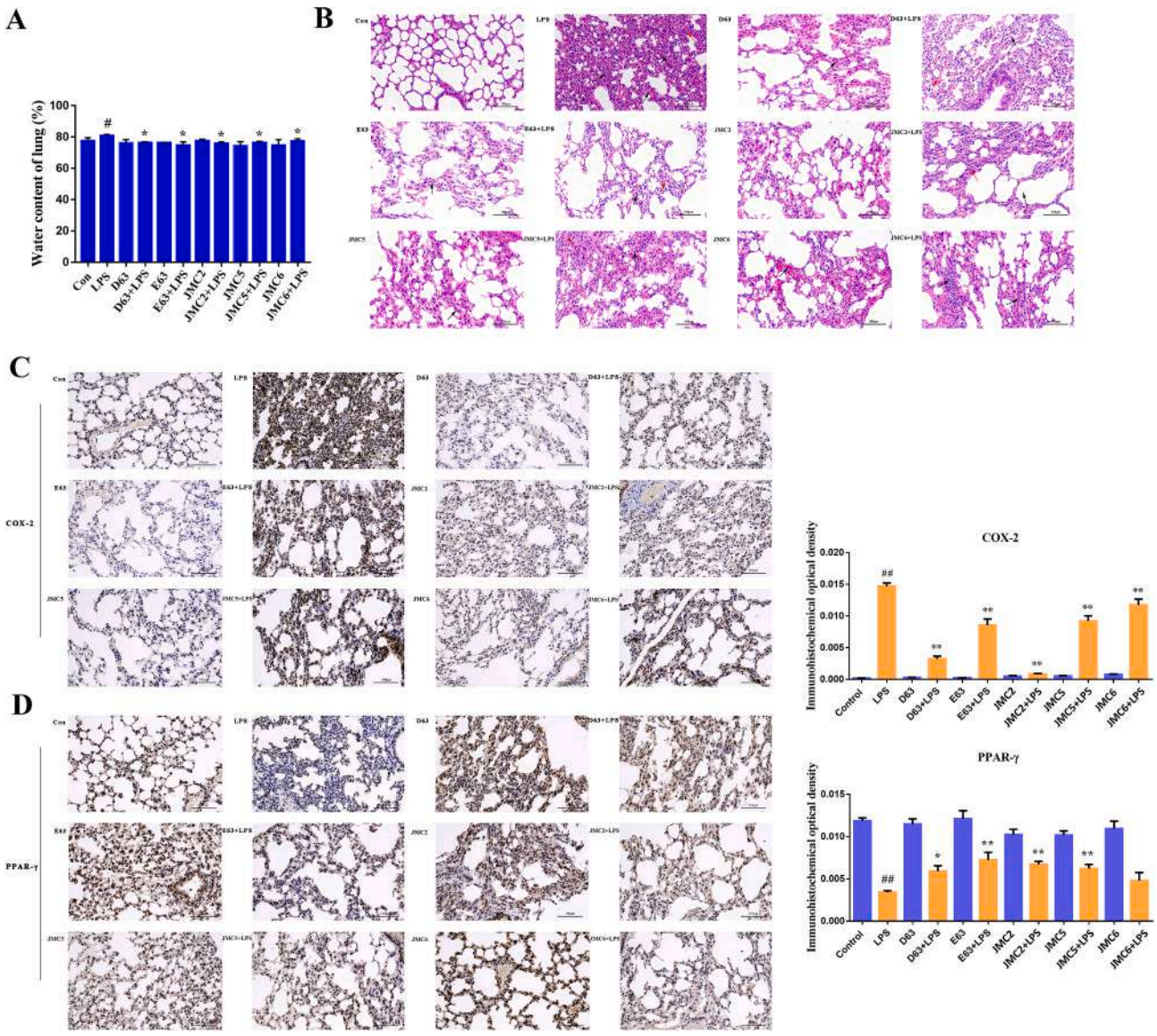

Fig. 10. The therapeutic effects of novel analogues on LPS-induced ALI in mice. Novel analogues significantly inhibited LPS-induced pulmonary oedema in mice (A). Inhibitory effect of novel analogues on LPS-induced lung injury by histopathology in mice (B). Changes in COX-2 and PPAR-γ in lung tissues of mice by immunohistochemistry (C, D). Statistical analysis was conducted by one-way ANOVA followed by Bonferroni's for multiple comparisons. All experiments were repeated in triplicate and data were represented as the mean ± SD from a represent experiments (n = 8). $\#p < 0.05$, $\#\#p < 0.01$ *vs* control group and LPS group; $*p < 0.05$, $**p < 0.01$ *vs* LPS group + different conditions group.

that members of the novel analogue group have therapeutic effects in lung injury induced by LPS. Further histopathological analysis of the lung tissue showed that the lung tissue structure of the LPS group was abnormal compared to the control group, with the thickening of some alveolar walls, alveolar atrophy and collapse, and lung parenchyma, as shown by the red arrow (Fig. 10B). Meanwhile, a large number of inflammatory cells could be seen in the lung parenchyma, and the inflammatory cells were dominated by neutrophils, as shown by the black arrow (Fig. 10B). The novel analogues alleviated the inflammatory damage induced by LPS to varying degrees, mainly manifested in a mild abnormal lung tissue structure, partial alveolar wall thickening and a small amount of inflammatory cell infiltration (Fig. 10B).

The COX-2 and PPAR-γ levels in the lung tissues were also assessed by immunohistochemical staining. The results showed that LPS can significantly increase COX-2 expression and decrease PPAR-γ expression, and that the novel analogues can attenuate the effects of LPS to varying degrees (Fig. 10C, D); a similar trend was observed with chemiluminescent Western blotting. Altogether, these results indicate that the novel analogues have the dual targeting effect of COX-2 and PPAR-γ, thus having the potential to treat LPS-induced ALI.

4. Discussion

The development of multi-target medicinal drugs is considered to be a key technology in drug research and development. Enhancing the effectiveness of medicines and employing multi-target anti-inflammatory drugs have emerged as promising therapeutic approaches for treating inflammation-related multifactorial diseases [1]. However, multi-target based medicinal drug design and multi-target screening strategies for medicinal drugs have not been fully established, which is one of the reasons for the hindered progress of medicinal drug discovery. ALI is known to be a cause of acute respiratory failure, characterised by a systemic inflammatory state and multifactorial induction, and is associated with higher mortality in patients of all ages [41]. However, current treatments still cannot significantly reduce the lung injury and mortality of ALI. The development and use of multi-target NSAID drugs

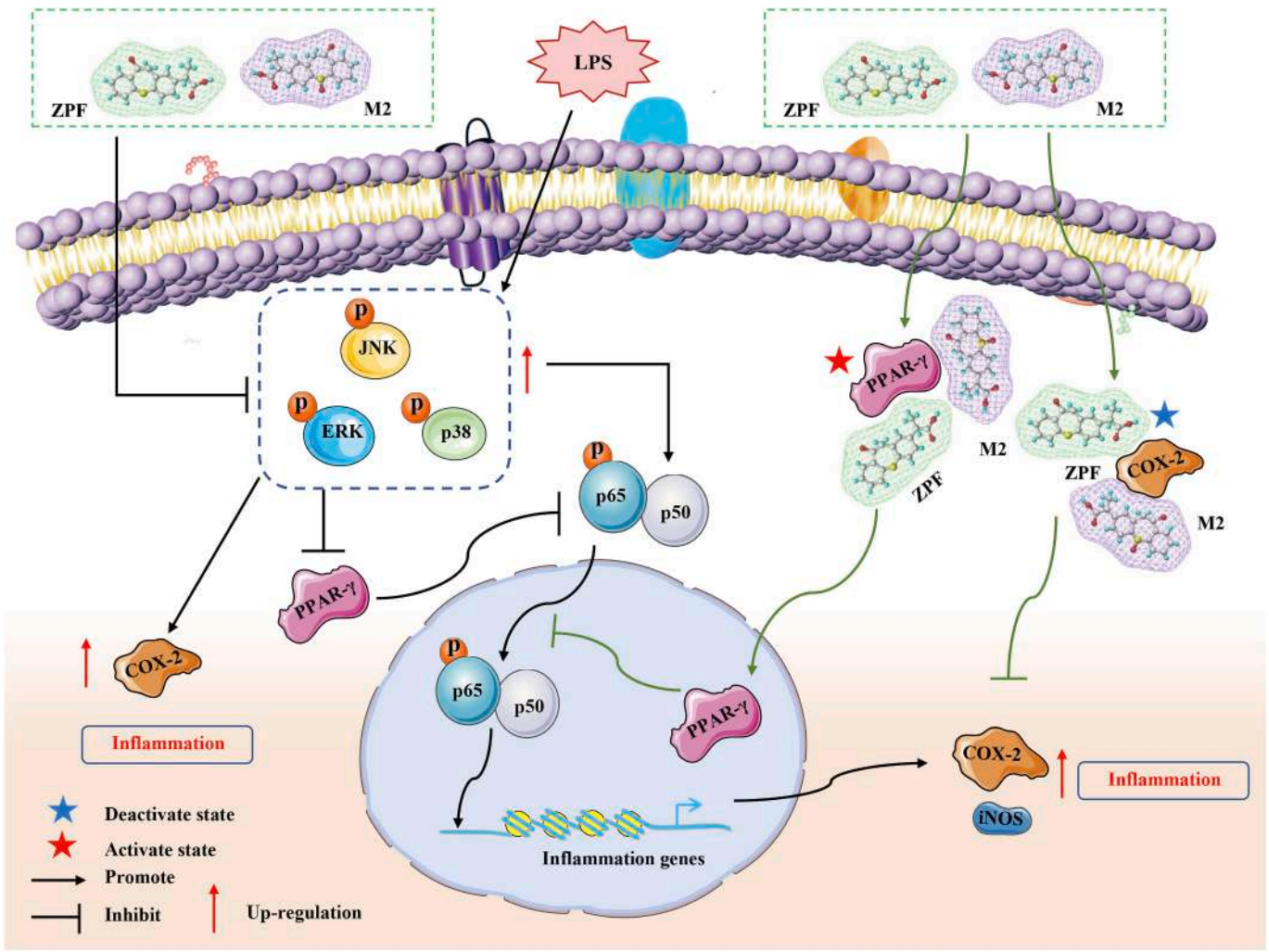

Fig. 11. The possible mechanisms of COX-2 and PPAR-γ may be effective dual targets for the treatment of LPS-induced ALI. On the one hand, ZPF and its metabolite M2 can inhibit the activity of COX-2 and activate the activity of PPAR-γ by binding with COX-2 and PPAR-γ, and further play an anti-inflammatory role. On the other hand, ZPF and its metabolite M2 can inhibit the LPS-induced inflammatory response through the MAPK-PPAR-γ/NF-κB signalling pathway.

may be an effective strategy for treating ALI patients with multiple inflammatory factors, as new and effective treatment strategies remain crucial for ALI patients. The STSBPT strategy was therefore developed and used to further confirm the multi-target NSAID effect of ZPF, its metabolite M2 and novel analogues, and to explore the therapeutic effect in the treatment of ALI. The results of *in vivo* and *in vitro* assays in this study show that ZPF, M2 and novel analogues have potential therapeutic effects on ALI by utilising the dual anti-inflammatory molecular target effect of PPAR-γ and COX-2 (Fig. 11).

The evaluation criteria for the STSBPT strategy primarily focus on two considerations. Firstly, the spatial density overlaps of the area of the active pockets: the larger the overlap area, the higher the similarity of the spatial structure. Secondly, the spatial directivity of key amino acids bound by the ligand and active pocket tends to be in the same direction, suggesting that the similarity of the active region of the active pocket is higher. However, the evaluation criteria are only considered from a qualitative point of view, and there is a lack of supporting calculation methods to enable quantitative analysis to be undertaken. It is therefore worth developing corresponding calculation strategies in the future to address this loophole.

The STSBPT strategy is an effective approach for exploring multi-target drugs. This strategy is mainly based on two considerations. Firstly, many medicines have a common single target activity pocket. For example, a new class of compounds has been identified using high-throughput screening techniques through the binding ability of COX enzyme activity pockets, further demonstrating the therapeutic effects of these compounds on pain and inflammation [42,43]. A group of COX-2 inhibitors designed using the active pocket of COX-2have been shown to elevate anti-inflammatory-analgesic activities *in vitro* and *in vivo* [44,45]. The above research studies indicate that multiple compounds can be designed to exhibit similar activities through the same active pocket on the same target. Secondly, the same medicines have a different protein target property, which means that they have multiple target activity pockets. For example, 6-(piperidin-1-ylsulfonyl)–2H-chromenes and 6-sulfonamide-2H-chromene derivatives targeting α-glucosidase, α-amylase, and PPAR-γ were discovered through the design, synthesis, virtual screening, and antidiabetic activity of compounds [46,47]. Moreover, a selective COX-2 inhibitor, indomethacin, can target Shr (Src homology 2-containing transforming protein)-EGFP (epidermal growth factor receptor), thereby inhibiting the MAPK signalling pathway [48,49]. Indomethacin functions as a PPAR-γ ligand by binding to the PPAR-γ ligand-binding domain, which in turn enhances the transcriptional activity of PPAR-γ [50]. In this research study, the STSBPT strategy combined with PyMOL software were employed to analyse the active pockets of indomethacin binding to COX-2 (PDB ID 5IKQ) and PPAR-γ (PDB ID 4XUM); the results showed that the active pockets of indomethacin binding to COX-2 and PPAR-γ had a certain degree of spatial similarity (Fig. 12). The above results indicate that the

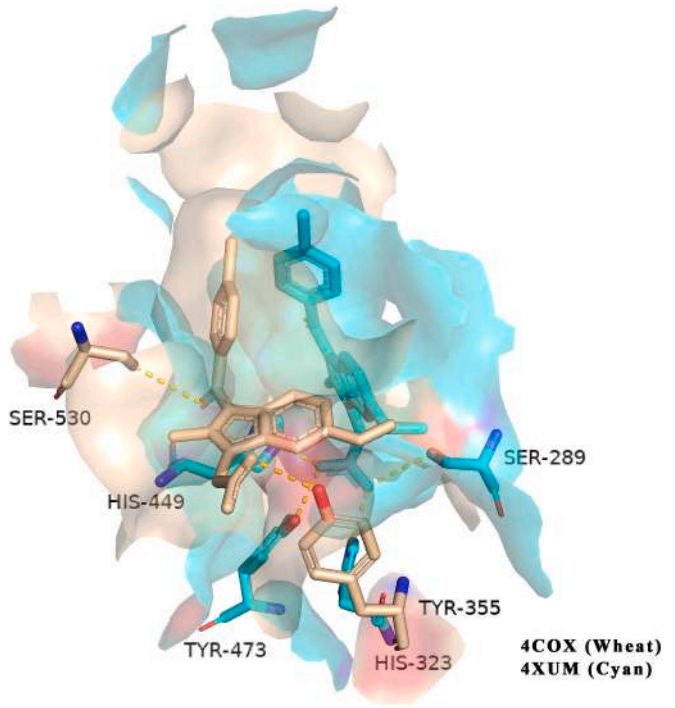

Fig. 12. Spatial similarity of indomethacin with COX-2 and PPAR-γ binding pockets was analysed based on the STSBPT strategy. Based on the STSBPT strategy and PyMOL software, the active pockets of indomethacin binding to COX-2 (PDB ID 4COX) and PPAR-γ (PDB ID 4XUM) were analysed, and the results showed a certain spatial similarity, which is mainly reflected in the higher spatial overlap region of the active pockets and the consistent spatial orientation of the key AA residues bound by indomethacin and active pockets of COX-2 and PPAR-γ.

drug indomethacin has a multi-target effect when exerting its efficacy and further proves the feasibility of the STSBPT strategy. Therefore, the STSBPT strategy was used to analyse the targeting of ZPF and its metabolite M2 to a range of inflammasome-related targets, such as PPAR-γ, NLRP3 and TLR4-MD2. ZPF and metabolite M2 were found to have the potential to target PPAR-γ in addition to COX-2. Notably, the present research study further developed more effective novel analogues with dual target effects based on the active pocket topology of ZPF and metabolite M2 with target proteins *in vitro* and *in vivo*.

Considering that most medicinal drugs are metabolised in the body, it is important to predict the metabolite targets based on the STSBPT strategy, as this can also help to predict the pharmacological activity of new medicines by metabolites in the body in advance. Meanwhile, the STSBPT strategy combined with molecular docking has an advantage in the development of new medicines. Hence, the present research study also compared the COX-1 binding ability of ZPF, metabolite M2 and novel analogues with mofezolac, the gastrointestinal toxicity of which works by inhibiting COX-1 activity [13]. ZPF, M2 and the novel analogues did not have the binding ability of mofezolac with COX-1, to inhibit COX-1 activity, and may not have a gastrointestinal toxicity similar to mofezolac. It is worth noting that the high resolution protein crystal structure and the development of precise simulations of drug-protein interactions, such as the application of artificial intelligence technology, can promote a further improvement of the STSBPT strategy, enabling the faster and more accurate detection of drug multiple target effects.

The application of multi-target drugs may be an effective strategy to resolve the multifactor inflammatory injury of ALI. Although the understanding of the pathophysiology of ALI has improved greatly over the past few decades, the mortality rate remains high and the efficacy of standard treatments is limited. The clinical treatment of ALI mainly involves the application of lung protective mechanical ventilation and some medicinal drugs, such as muscle blockers, corticosteroids, phosphodiesterase inhibitors and acetylsalicylic acid (aspirin), among others, but there is currently no significant and consistent specific pharmacotherapy for ALI [51]. This may be due to the complex pathological mechanism of ALI, whereby targeting a single pathogenesis or target is not an effective therapy [51]. Except for COX-2 target, in this research study, the STSBPT strategy was developed and used to screen another key anti-inflammatory target of ZPF, M2, PPAR-γ, which was further full validated by CETSA, DARTS, and the *in vitro* and *in vivo* assays. Based on the dual targets of COX-2 and PPAR-γ, the STSBPT strategy was applied to design novel analogues, which were found to have stronger drug efficacy against LPS-induced ALI.

COX-2 and PPAR-γ serve as effective dual targets of ZPF, its metabolite M2 and its analogues for treating inflammation in ALI. For example, Norwogonin attenuates LPS-induced ALI by inhibiting the Src/AKT1/NF-κB signaling pathway through direct targeting of Src, AKT1 and COX-2 [52]. Kirenol ameliorates endotoxin-induced ALI by inhibiting COX-2 expression and the ERK and JNK phosphorylation-mediated NF-κB pathway in mice [53]. Moreover, ACT001 (a derivative of michelolide from the natural product parthenolide) alleviates inflammation and pyroptosis through the PPAR-γ/NF-κB signalling pathway in LPS-induced ALI model [54]. The current study also found that ZPF, M2 and its novel analogues can, on the one hand, play a role in resisting LPS-induced inflammatory responses through the MAPK/PPAR-γ/NF-κB signalling pathway, and on the other hand, play an anti-inflammatory role by binding to COX-2 and PPAR-γ, playing an inhibitory and activating role, respectively. Altogether, the present research study not only demonstrates that ZPF, the metabolite M2 and the novel analogues exert protection against ALI through PPAR-γ and COX-2, but also demonstrates the feasibility of the STSBPT strategy by proving the verification between drugs and multi-targets from a virtual setting through to reality. However, further research studies should be carried out in the future. Firstly, compounds identified by STSBPT need to be benchmarked against existing therapeutics to assess whether dual functionality indeed enhances the anti-inflammatory effects. Secondly, it is not clear if the achieved *in vivo* pharmacokinetics/pharmacodynamics permitted the observed dual action of these compounds *in vitro*. Thirdly, it remains to be further evaluated how these compounds target COX-2/PPAR-γ to ameliorate LPS-induced ALI.

In summary, the present data suggests that the STSBPT strategy could serve as an effective approach for designing and selecting multi-target medicinal drugs. Meanwhile, based on the STSBPT strategy, the potential of ZPF, the metabolite M2 and novel analogues has been demonstrated *in vitro* and *in vivo* in the treatment of LPS-induced ALI.

CRediT authorship contribution statement

Qirong Lu: Writing – review & editing, Formal analysis, Methodology, Data curation, Investigation. **Yongxia Zhao:** Investigation, Writing – review & editing, Formal analysis, Methodology, Data curation. **Xiaoqing Xu:** Methodology, Data curation, Investigation, Writing – review & editing, Formal analysis. **Pu Guo:** Writing – review & editing, Formal analysis, Methodology, Data curation, Investigation. **Irma Ares:** Investigation, Writing – review & editing, Formal analysis, Methodology, Data curation. **Marta Martínez:** Methodology, Data curation, Investigation, Writing – review & editing, Formal analysis. **Bernardo Lopez-Torres:** Writing – review & editing, Formal analysis, Methodology, Data curation, Investigation. **María-Rosa Martínez-Larrañaga:** Investigation, Writing – review & editing, Formal analysis, Methodology, Data curation. **Arturo Anadón:** Writing – review & editing, Funding acquisition, Conceptualization, Writing – original draft, Formal analysis, Project administration, Data curation. **Yuanhu Pan:** Writing – original draft, Formal analysis, Project administration, Data curation, Writing – review & editing, Funding acquisition, Conceptualization. **Xu Wang:** Project administration, Data curation, Writing – review &

editing, Funding acquisition, Conceptualization, Writing – original draft, Formal analysis. **María-Aránzazu Martínez:** Project administration, Data curation, Writing – review & editing, Funding acquisition, Conceptualization, Writing – original draft, Formal analysis.

Declaration of competing interest

The authors declare that they have no known competing financial interests or personal relationships that could have appeared to influence the work reported in this paper.

Acknowledgements

This work was supported by National Natural Science Foundation of China (NSFC) (32473087), National Key Research and Development Program of China (2017YFD0501401) and Fundamental Research Funds for the Central Universities (2662020DKPY020), and Project Ref. PID 2020-115979RR-C33 from Ministerio de Ciencia e Innovación, Spain (Project/AEI/10.13039/501100011033). We thank Dr. Heying Zhang and Dr. Bo Zhou for their guidance in chemical synthesis.

Data availability

Data will be made available on request.

References

[1] L. Costantino, D. Barlocco, Challenges in the design of multitarget drugs against multifactorial pathologies: a new life for medicinal chemistry? Future Med. Chem. 5 (2013) 5–7, https://doi.org/10.4155/fmc.12.193.
[2] B.L. Roth, D.J. Sheffler, W.K. Kroeze, Magic shotguns versus magic bullets: selectively non-selective drugs for mood disorders and schizophrenia, Nat. Rev. Drug Discov. 3 (2004) 353–359, https://doi.org/10.1038/nrd1346.
[3] G. Kaur, O. Silakari, Multiple target-centric strategy to tame inflammation, Future, Med. Chem. 9 (2017) 1361–1376, https://doi.org/10.4155/fmc-2017-0050.
[4] P. Csermely, V. Ágoston, S. Pongor, The efficiency of multi-target drugs: the network approach might help drug design, Trends Pharmacol. Sci. 26 (2005) 178–182, https://doi.org/10.1016/j.tips.2005.02.007.
[5] T. Hase, H. Tanaka, Y. Suzuki, S. Nakagawa, H. Kitano, Structure of protein interaction networks and their implications on drug design, PLoS Comput. Biol. 5 (2009) e1000550, https://doi.org/10.1371/journal.pcbi.1000550.
[6] A. Cavalli, M.L. Bolognesi, A. Minarini, M. Rosini, V. Tumiatti, M. Recanatini, C. Melchiorre, Multi-target-directed ligands to combat neurodegenerative diseases, J. Med. Chem. 51 (2008) 347–372, https://doi.org/10.1021/jm7009364.
[7] D. Singh, Merck withdraws arthritis drug worldwide, BMJ 329 (2004) 816, https://doi.org/10.1136/bmj.329.7470.816-a.
[8] J.M. Alvaro-Gracia, Licofelone-clinical update on a novel LOX/COX inhibitor for the treatment of osteoarthritis, Rheumatology 43 (2004) i21–i25, https://doi.org/10.1093/rheumatology/keh105.
[9] H.H. Yang, J.X. Duan, S.K. Liu, J.B. Xiong, X.X. Guan, W.J. Zhong, C.C. Sun, C. Y. Zhang, X.Q. Luo, Y.F. Zhang, P. Chen, B.D. Hammock, S.H. Hwang, J.X. Jiang, Y. Zhou, C.X. Guan, A COX-2/sEH dual inhibitor PTUPB alleviates lipopolysaccharide-induced acute lung injury in mice by inhibiting NLRP3 inflammasome activation, Theranostics 10 (2020) 4749–4761, https://doi.org/10.7150/thno.43108.
[10] C.Y. Huang, J.S. Deng, W.C. Huang, W.P. Jiang, G.J. Huang, Attenuation of lipopolysaccharide-induced acute lung injury by hispolon in mice, through regulating the TLR4/PI3K/Akt/mTOR and Keap1/Nrf2/HO-1 pathways, and suppressing oxidative stress-mediated ER stress-induced apoptosis and autophagy, Nutrients 12 (2020) 1742, https://doi.org/10.3390/nu12061742.
[11] M.A. Matthay, R.L. Zemans, G.A. Zimmerman, Y.M. Arabi, J.R. Beitler, A. Mercat, M. Herridge, A.G. Randolph, C.S. Calfee, Acute respiratory distress syndrome, Nat. Rev. Dis. Primers 5 (2019) 18, https://doi.org/10.1038/s41572-019-0069-0.
[12] Y. Hu, J. Lou, Y.Y. Mao, T.W. Lai, L.Y. Liu, C. Zhu, C. Zhang, J. Liu, Y.Y. Li, F. Zhang, W. Li, S.M. Ying, Z.H. Chen, H.H. Shen, Activation of MTOR in pulmonary epithelium promotes LPS-induced acute lung injury, Autophagy 12 (2016) 2286–2299, https://doi.org/10.1080/15548627.2016.1230584.
[13] A. Ito, Y. Mori, Effect of a novel anti-inflammatory drug, 2-(10, 11-dihydro-10-oxo-dibenzo[b,f]-thiepin-2-yl)propionic acid (CN-100), on the proteoglycan biosynthesis in articular chondrocytes and prostaglandin E2 production in synovial fibroblasts, Res. Commun. Chem. Pathol. Pharmacol. 70 (1990) 131–142. PMID: 2177561.
[14] K. Sasaki, K. Iizuka, H. Sano, M. Miwa, S. Harnki, Pharmacokinetics of CN-100 for 80 mg tablet of final preparation in healthy volunteers, Jpn. Pharmacol. Ther. 20 (1992) 2167–2174.
[15] K. Hirate, A. Uchida, Y. Ogawa, T. Arai, K. Yoda, Zaltoprofen, a non-steroidal anti-inflammatory drug, inhibits bradykinin-induced pain responses without blocking bradykinin receptors, Neurosci. Res. 54 (2006) 288–294, https://doi.org/10.1016/j.neures.2005.12.016.
[16] T. Okamoto, NSAID zaltoprofen improves the decrease in body weight in rodent sickness behavior models: proposed new applications of NSAIDs (Review), Int. J. Mol. Med. 9 (2002) 369–372, https://doi.org/10.3892/ijmm.9.4.369.
[17] K. Tsurumi, K. Kyuki, M. Niwa, H. Mibu, H. Fujimura, Pharmacological investigations of the new antiinflammatory agent 2-(10,11-dihydro-10-oxodibenzo [b,f]thiepin-2-yl)propionic acid. 2nd communication: inhibitory effects on acute inflammation and prostaglandin-related reactions, Arzneimittelforschung 36 (1986) 1801–1805. PMID: 3105545.
[18] K.P. Steinberg, L.D. Hudson, R.B. Goodman, C.L. Hough, P.N. Lanken, R. Hyzy, B. T. Thompson, M. Ancukiewicz, National Heart, Lung, and Blood Institute Acute Respiratory Distress Syndrome (ARDS) Clinical Trials Network, Efficacy and safety of corticosteroids for persistent acute respiratory distress syndrome, N. Engl. J. Med. 354 (2006) 1671–1684, https://doi.org/10.1056/NEJMoa051693.
[19] L. Gattinoni, P. Caironi, M. Cressoni, D. Chiumello, V.M. Ranieri, M. Quintel, S. Russo, N. Patroniti, R. Cornejo, G. Bugedo, Lung recruitment in patients with the acute respiratory distress syndrome, N. Engl. J. Med. 354 (2006) 1775–1786, https://doi.org/10.1056/NEJMoa052052.
[20] K. Sindelár, B. Kakác, J. Metysová, M. Protiva, Neurotropic and psychotropic agents: 9-chloro-10-(4-methylpiperazino)-10,11-dihydrodibenzo(b,f)thiepin. (preliminary communication), Farmaco Sci. 28 (1973) 256–261. PMID: 4693634.
[21] E. Bergamaschi, D. Lunic, L.A. McLean, M. Hohenadel, Y.K. Chen, C.J. Teskey, Controlling chemoselectivity of catalytic hydroboration with light, Angew. Chem. Int. Ed. 61 (2022) e202114482, https://doi.org/10.1002/anie.202114482.
[22] D. Hands, H. Marley, S.J. Skittrall, S.H.B. Wright, T.R. Verhoeven, The synthesis of 3-hydroxymethyldibenzo[b,f]thiepin 5,5-dioxide, a prostaglandin antagonist, J. Heterocycl. Chem. 23 (1986) 1333–1337, https://doi.org/10.1002/jhet.5570230513.
[23] K.I. Awasaguchi, H. Hayashi, H. Kawai, H. Tominaga, Y. Sato, K. Hayashi, Y. Todo, Synthetic protocols mutually applicable to 4-oxoquinolines and 4-oxo-1,8-naphthyridines: synthesis of 1-aryl-2-substituted and 1-aryl-3-fluoro-4-oxoquinolines and 4-oxo-1,8-naphthyridines, Synlett 23 (2012) 448–452, https://doi.org/10.1055/s-0031-1290079.
[24] L. Cheng, M.M. Li, B. Wang, L.J. Xiao, J.H. Xie, Q.L. Zhou, Nickel-catalyzed hydroalkylation and hydroalkenylation of 1,3-dienes with hydrazones, Chem. Sci. 10 (2019) 10417–10421, https://doi.org/10.1039/c9sc04177j.
[25] M. Ueda, H. Mori, Diphenyl (2,3-dihydro-2-thioxo-3-benzoxazolyl)phosphonate: a new, reactive condensing agent for the synthesis of amides, esters, peptides, and β-lactams via condensation, Bull. Chem. Soc. Jpn. 65 (1992) 1636–1641, https://doi.org/10.1246/bcsj.65.1636.
[26] M. Matsugi, M. Hasegawa, D. Sadachika, S. Okamoto, M. Tomioka, Y. Ikeya, A. Masuyama, Y. Mori, Preparation and condensation reactions of a new light-fluorous Mukaiyama reagent: reliable purification with fluorous solid phase extraction for esters and amides, Tetrahedron Lett. 48 (2007) 4147–4150, https://doi.org/10.1016/j.tetlet.2007.03.173.
[27] X. Xiang, X. Xin, Y. Hou, Y. Deng, X. Liu, W. Yu, Diosgenin alters LPS-induced macrophage polarization by activating PPARγ/NF-κB signaling pathway, Int. Immunopharmacol. 126 (2024) 111270, https://doi.org/10.1016/j.intimp.2023.111270.
[28] J. Zhou, B. Lei, H. Li, L. Zhu, L. Wang, H. Tao, S. Mei, F. Li, MicroRNA-144 is regulated by CP2 and decreases COX-2 expression and PGE2 production in mouse ovarian granulosa cells, Cell Death Dis. 8 (2017) e2597.
[29] M. Hawash, N. Jaradat, R. Sabobeh, M. Abualhasan, M.T. Qaoud, New thiazole carboxamide derivatives as COX inhibitors: design, synthesis, anticancer screening, in silico molecular docking, and ADME profile studies, ACS Omega 8 (2023) 29512–29526, https://doi.org/10.1021/acsomega.3c03256.
[30] LLC. Schrödinger, The PyMOL molecular graphics system, version 1.8, Schrödinger, LLC; New York, USA (2015).
[31] P.C. Ng, S. Henikoff, SIFT: predicting amino acid changes that affect protein function, Nucleic Acids Res. 31 (2003) 3812–3814, https://doi.org/10.1093/nar/gkg509.
[32] I. Adzhubei, D.M. Jordan, S.R. Sunyaev, Predicting functional effect of human missense mutations using PolyPhen-2, Curr. Protoc. Hum. Genet. 76 (2013) 7.20.1-7.20.41, https://doi.org/10.1002/0471142905.hg0720s76.
[33] J. Ning, S. Ahmed, G. Cheng, T. Chen, Y. Wang, D. Peng, Z. Yuan, Analysis of the stability and affinity of BlaR-CTD protein to β-lactam antibiotics based on docking and mutagenesis studies, J. Biol. Eng. 13 (2019) 27, https://doi.org/10.1186/s13036-019-0157-4.
[34] E.W. Ehrich, A. Dallob, I. De Lepeleire, A. Van Hecken, D. Riendeau, W. Yuan, A. Porras, J. Wittreich, J.R. Seibold, P. De Schepper, D.R. Mehlisch, B.J. Gertz, Characterization of rofecoxib as a cyclooxygenase-2 isoform inhibitor and demonstration of analgesia in the dental pain model, Clin. Pharmacol. Ther. 65 (1999) 336–347, https://doi.org/10.1016/S0009-9236(99)70113-X.
[35] M.Y. Pai, B. Lomenick, H. Hwang, R. Schiestl, W. McBride, J.A. Loo, J. Huang, Drug affinity responsive target stability (DARTS) for small-molecule target identification, in: J.E. Hempel, C.H. Williams, C.C. Hong (Eds.), Chemical Biology. Methods and Protocols, Humana Press, New York, 2015, pp. 287–298, https://doi.org/10.1007/978-1-4939-2269-7_22.
[36] N. Murakami, H. Takase, T. Tomita, K. Iwata, T. Naruse, Antinociceptive activity of a novel non-steroidal anti-inflammatory drug (M-5011) with low ulcerogenic effects in mice, Jpn. J. Pharmacol. 72 (1996) 29–37, https://doi.org/10.1254/jjp.72.29.
[37] Y.Y. Yu, X.Q. Li, W.P. Hu, S.C. Cu, J.J. Dai, Y.N. Gao, Y.T. Zhang, X.Y. Bai, D.Y. Shi, Self-developed NF-κB inhibitor 270 protects against LPS-induced acute kidney

injury and lung injury through improving inflammation, Biomed. Pharmacother. 147 (2022) 112615, https://doi.org/10.1016/j.biopha.2022.112615.
[38] K.F. Alsharif, A.A. Almalki, W.F. Alsanie, K.J. Alzahrani, S.M. Kabrah, G. E. Elshopakey, A.A.A. Alghamdi, M.S. Lokman, H.A. Sberi, A.A. Bauomy, A. Albrakati, S.S. Ramadan, R.B. Kassab, A.E. Abdel Moneim, F.E.H. Salem, Protocatechuic acid attenuates lipopolysaccharide-induced septic lung injury in mice: the possible role through suppressing oxidative stress, inflammation and apoptosis, J. Food Biochem. 45 (2021) e13915, https://doi.org/10.1111/jfbc.13915.
[39] A.K. Reka, M.T. Goswami, R. Krishnapuram, T.J. Standiford, V.G. Keshamouni, Molecular cross-regulation between PPAR-γ and other signaling pathways: implications for lung cancer therapy, Lung Cancer 72 (2011) 154–159, https://doi.org/10.1016/j.lungcan.2011.01.019.
[40] W. Zhu, H. Yan, S. Li, W. Nie, F. Fan, J. Zhu, PPAR-γ agonist pioglitazone regulates dendritic cells immunogenicity mediated by DC-SIGN via the MAPK and NF-κB pathways, Int. Immunopharmacol. 41 (2016) 24–34, https://doi.org/10.1016/j.intimp.2016.09.028.
[41] J. Yao, D. Pan, Y. Zhao, L. Zhao, J. Sun, Y. Wang, Q.D. You, T. Xi, Q.L. Guo, N. Lu, Wogonin prevents lipopolysaccharide-induced acute lung injury and inflammation in mice via peroxisome proliferator-activated receptor gamma-mediated attenuation of the nuclear factor-kappaB pathway, Immunology 143 (2014) 241–257, https://doi.org/10.1111/imm.12305.
[42] J. Gierse, M. Nickols, K. Leahy, J. Warner, Y. Zhang, L. Cortes-Burgos, J. Carter, K. Seibert, J. Masferrer, Evaluation of COX-1/COX-2 selectivity and potency of a new class of COX-2 inhibitors, Eur. J. Pharmacol. 588 (2008) 93–98, https://doi.org/10.1016/j.ejphar.2008.03.057.
[43] R. Ayman, M.S. Abusaif, A.M. Radwan, A.M. Elmetwally, A. Ragab, Development of novel pyrazole, imidazo[1,2-b]pyrazole, and pyrazolo[1,5-a]pyrimidine derivatives as a new class of COX-2 inhibitors with immunomodulatory potential, Eur. J. Med. Chem. 249 (2023) 115138, https://doi.org/10.1016/j.ejmech.2023.115138.
[44] P.N. Praveen Rao, M. Amini, H. Li, A.G. Habeeb, E.E. Knaus, Design, synthesis, and biological evaluation of 6-substituted-3-(4-methanesulfonylphenyl)-4-phenyl-pyran-2-ones: a novel class of diarylheterocyclic selective cyclooxygenase-2 inhibitors, J. Med. Chem. 46 (2003) 4872–4882, https://doi.org/10.1021/jm0302391.
[45] A. Ragab, R. Ayman, M.A. Salem, Y.A. Ammar, M.S. Abusaif, Unveiling a novel pyrazolopyrimidine scaffold as a dual COX-2/5-LOX inhibitor with immunomodulatory potential: design, synthesis, target prediction, anti-inflammatory activity, and ADME-T with docking simulation, Eur. J. Med. Chem. 290 (2025) 117499, https://doi.org/10.1016/j.ejmech.2025.117499.
[46] H.K. Thabet, M.S. Abusaif, M. Imran, M.H. Helal, S.I. Alaqel, A. Alshehri, A. A. Mohd, Y.A. Ammar, A. Ragab, Discovery of novel 6-(piperidin-1-ylsulfonyl)-2H-chromenes targeting α-glucosidase, α-amylase, and PPAR-γ: design, synthesis, virtual screening, and anti-diabetic activity for type 2 diabetes mellitus, Comput. Biol. Chem. 111 (2024) 108097, https://doi.org/10.1016/j.compbiolchem.2024.108097.
[47] H.K. Thabet, A. Ragab, M. Imran, M. Hamdy Helal, S. Ibrahim Alaqel, A. Alshehri, A. Ash Mohd, S.S. Alshammari, Y.A. Ammar, M.S. Abusaif, Innovation of 6-sulfonamide-2H-chromene derivatives as antidiabetic agents targeting α-amylase, α-glycosidase, and PPAR-γ inhibitors with in silico molecular docking simulation, RSC Adv. 14 (2024) 15691–15705, https://doi.org/10.1039/d4ra02143f.
[48] C.C. Lin, K.M. Suen, A. Stainthorp, L. Wieteska, G.S. Biggs, A. Leitão, C. A. Montanari, J.E. Ladbury, Targeting the Shc-EGFR interaction with indomethacin inhibits MAP kinase pathway signalling, Cancer Lett. 457 (2019) 86–97, https://doi.org/10.1016/j.canlet.2019.05.008.
[49] R.G. Kurumbail, A.M. Stevens, J.K. Gierse, J.J. McDonald, R.A. Stegeman, J.Y. Pak, D. Gildehaus, J.M. Miyashiro, T.D. Penning, K. Seibert, P.C. Isakson, W.C. Stallings, Structural basis for selective inhibition of cyclooxygenase-2 by anti-inflammatory agents, Nature 384 (1996) 644–648, https://doi.org/10.1038/384644a0.
[50] A.C. Puhl, F.A. Milton, A. Cvoro, D.H. Sieglaff, J.C.L. Campos, A. Bernardes, C. S. Filgueira, J.L. Lindemann, T. Deng, F.A.R. Neves, I. Polikarpov, P. Webb, Mechanisms of peroxisome proliferator activated receptor γ regulation by non-steroidal anti-inflammatory drugs, Nucl. Recep. Signal. 13 (2015) e004.
[51] D. Mokrá, Acute lung injury-from pathophysiology to treatment, Physiol. Res. 69 (2020) S353–S366. https://doi.org/10.33549/physiolres.934602.
[52] T. Cao, A.Q. Li, Y. Zhang, T.T. Xie, D.Z. Weng, C.S. Pan, L. Yan, K. Sun, D. Wang, J. Y. Han, J. Liu, Norwogonin attenuates LPS-induced acute lung injury through inhibiting Src/AKT1/NF-κB signaling pathway, Phytomedicine 139 (2025) 156432, https://doi.org/10.1016/j.phymed.2025.156432.
[53] F.C. Lin, S.P. Chen, S.C. Lin, C.C. Tseng, S.C. Tsai, Y.H. Kuan, Kirenol ameliorates endotoxin-induced acute lung injury by inhibiting the ERK and JNK phosphorylation-mediated NFκB pathway in mice, Inflammopharmacology 33 (2025) 2069–2081, https://doi.org/10.1007/s10787-025-01693-2.
[54] Q. Fu, N. Shen, T. Fang, H. Zhang, Y. Di, X. Liu, C. Du, J. Guo, ACT001 alleviates inflammation and pyroptosis through the PPAR-γ/NF-κB signaling pathway in LPS-induced alveolar macrophages, Genes Genom. 46 (2024) 323–332, https://doi.org/10.1007/s13258-023-01455-w.